

# Lawrence Berkeley National Laboratory

## Lawrence Berkeley National Laboratory

### Title

Reaction of the C<sub>2</sub>H radical with 1-butyne (C<sub>4</sub>H<sub>6</sub>): Low Temperature Kinetics and Isomer-Specific Product Detection

### Permalink

<https://escholarship.org/uc/item/93p90905>

### Author

Soorkia, Satchin

### Publication Date

2010-03-03

Peer reviewed

1  
2  
3  
4  
5  
6  
7  
8  
9

**Reaction of the C<sub>2</sub>H radical with 1-butyne (C<sub>4</sub>H<sub>6</sub>):**  
**Low temperature kinetics and isomer-specific product detection**

10 Satchin Soorkia<sup>a</sup>, Adam J. Trevitt<sup>b</sup>, Talitha M. Selby<sup>c</sup>, David L. Osborn<sup>d</sup>, Craig A. Taatjes<sup>d</sup>,  
11  
12 Kevin R. Wilson<sup>c</sup> and Stephen R. Leone<sup>a,e,\*</sup>  
13

14  
15 <sup>a</sup>Departments of Chemistry and Physics, University of California, Berkeley, California 94720,  
16 USA  
17

18 <sup>b</sup>School of Chemistry, University of Wollongong, New South Wales 2522, Australia

19 <sup>c</sup>Department of Chemistry, University of Wisconsin – Washington County, West Bend, WI  
20  
21 53095, USA  
22

23 <sup>d</sup>Combustion Research Facility, Mail Stop 9055, Sandia National Laboratories, Livermore, CA  
24  
25 94551-0969, USA  
26

27 <sup>e</sup>Chemical Sciences Division, Lawrence Berkeley National Laboratory, 1 Cyclotron Road,  
28  
29 Berkeley, CA 94720, USA  
30

31  
32  
33 \*On appointment as a Miller Research Professor in the Miller Institute for Basic Research in  
34  
35 Science  
36

37  
38 Electronic mail: srl@berkeley.edu  
39  
40  
41  
42  
43  
44  
45  
46  
47  
48  
49  
50  
51  
52  
53  
54  
55  
56  
57  
58  
59  
60

## Abstract

The rate coefficient for the reaction of the ethynyl radical ( $C_2H$ ) with 1-butyne ( $H-C\equiv C-CH_2-CH_3$ ) is measured in a pulsed Laval nozzle apparatus. Ethynyl radicals are formed by laser photolysis of acetylene ( $C_2H_2$ ) at 193 nm and detected *via* chemiluminescence ( $C_2H + O_2 \rightarrow CH(A^2\Delta) + CO_2$ ). The rate coefficients are measured over the temperature range of 74-295 K. The  $C_2H + 1$ -butyne reaction exhibits no barrier and occurs with rate constants close to the collision limit. The temperature dependent rate coefficients can be fit within experimental uncertainties by the expression  $k = (2.4 \pm 0.5) \times 10^{-10} (T/295 \text{ K})^{-(0.04 \pm 0.03)} \text{ cm}^3 \text{ molecule}^{-1} \text{ s}^{-1}$ . Reaction products are detected at room temperature (295 K) and 533 Pa using a Multiplexed Photoionization Mass Spectrometer (MPIMS) coupled to the tunable VUV synchrotron radiation from the Advanced Light Source at the Lawrence Berkeley National Laboratory. Two product channels are identified for this reaction:  $m/z = 64$  ( $C_5H_4$ ) and  $m/z = 78$  ( $C_6H_6$ ) corresponding to the  $CH_3$ - and H-loss channels, respectively. Photoionization efficiency (PIE) curves are used to analyze the isomeric composition of both product channels. The  $C_5H_4$  products are found to be exclusively linear isomers composed of ethynylallene and methylidyneacetylene in a 4:1 ratio. In contrast, the  $C_6H_6$  product channel includes two cyclic isomers, fulvene 18( $\pm$ 5)% and 3,4-dimethylenecyclobut-1-ene 32( $\pm$ 8)%, as well as three linear isomers, 2-ethynyl-1,3-butadiene 8( $\pm$ 5)%, 3,4-hexadiene-1-yne 28( $\pm$ 8)% and 1,3-hexadiyne 14( $\pm$ 5)%. Within experimental uncertainties, we do not see appreciable amounts of benzene and an upper limit of 10 % is estimated. Diacetylene ( $C_4H_2$ ) formation *via* the  $C_2H_5$ -loss channel is also thermodynamically possible but cannot be observed due to experimental limitations. The implications of these results for modeling of planetary atmospheres, especially of Saturn's largest moon Titan, are discussed.

## 1. Introduction

The ethynyl radical,  $C_2H$ , is an important polyatomic radical in the interstellar medium.<sup>1</sup> Its relative abundance is a marker of the carbon richness of its environment, as observed on Saturn's largest moon, Titan.  $C_2H$  radicals are formed in the cold, dense, structured and complex atmosphere of Titan<sup>2-4</sup> by the photolysis (*via* solar radiation) of acetylene.<sup>5</sup> Moreover, ethynyl radicals are believed to play a major role in the molecular weight growth of larger carbonaceous species. In a model proposed by Wilson and Atreya,<sup>6</sup> to account for the dense haze observed on Titan, the reaction of the  $C_2H$  radical with acetylene is a key step in the formation of longer chain polyynes molecules (e.g.  $C_4H_2$  and  $C_6H_2$ ). These polyynes can subsequently react further with  $C_2H$  radicals to eventually form much larger polymeric species that ultimately contribute to the observed photochemically active and colored organic haze.<sup>7</sup> Similarly,  $C_2H$  is a key radical in the formation of polycyclic aromatic hydrocarbons (PAHs),<sup>6</sup> which are believed to play an important role in interstellar chemistry.<sup>8,9</sup>

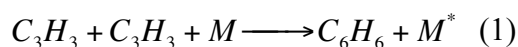
Benzene ( $C_6H_6$ ), the simplest aromatic hydrocarbon, is considered to be a precursor for larger PAH formation and its recent identification on Titan<sup>10</sup> strongly suggests that much more complex PAH synthesis may proceed in the cold atmosphere of the Saturnian moon. Recently, Mebel and coworkers<sup>11</sup> proposed a novel Ethynyl Addition Mechanism (EAM) as a viable alternative to the high-temperature Hydrogen-Abstraction- $C_2H_2$ -Addition (HACA)<sup>12</sup> mechanism for the formation of PAHs at very low temperatures. As described,<sup>11</sup> this mechanism is initiated by the addition of a  $C_2H$  radical to an ortho-carbon of ethynylbenzene ( $C_6H_5-C\equiv C-H$ ), and the reactive intermediate subsequently loses a H atom to form 1,2-diethynylbenzene. The latter then reacts with a second  $C_2H$  radical *via* addition to one of the carbon atoms on the ethynyl side chains. Ring closure of the intermediate leads to the formation of the ethynyl substituted bicyclic naphthalene core. The authors conclude that since the stepwise addition of  $C_2H$  radicals (followed by H atom elimination) to benzene, ethynylbenzene and 1,2-diethynylbenzene occurs without a barrier and with high exothermicity, the reactions of  $C_2H$  radicals should be very fast, and they suggest that the reactions should proceed with rate constants on the order of  $10^{-10} \text{ cm}^3 \text{ molecule}^{-1} \text{ s}^{-1}$  even at very low temperatures.

1  
2  
3  
4  
5 Since  $C_2H$  is a key species in carbon-rich environments, it has been the subject of a number of  
6 studies.<sup>11,13-26</sup> In order to analyze and account for the presence of hydrocarbon species, modeling  
7 studies are of central importance in understanding the complex nature of Titan's atmosphere.  
8 Detailed models have been developed over the last few decades.<sup>6,27,28</sup> Low temperature rate  
9 constants and product branching ratios are used when available to describe accurately and  
10 reliably<sup>29</sup> the chemical schemes<sup>27</sup> that are proposed. In this respect, much progress<sup>30</sup> has been  
11 made experimentally to obtain kinetic data on key chemical reactions down to very low  
12 temperatures relevant to interstellar chemistry. The CRESU (Cinétique de Réaction Chimique en  
13 Ecoulement Supersonique Uniforme) technique, pioneered by Rowe and coworkers,<sup>31,32</sup> involves  
14 the expansion of a gas mixture through a Laval nozzle and allows kinetic studies down to 10 K to  
15 examine chemistry under true interstellar conditions.<sup>31-35</sup> M. A. Smith and coworkers<sup>36,37</sup>  
16 developed a pulsed Laval apparatus that was adopted by Leone and coworkers<sup>21</sup> and Abel and  
17 coworkers.<sup>30</sup> The collimated supersonic flow generated by a Laval nozzle can be compared to a  
18 "wall-less flow tube reactor" in which reactions involving species with very low vapor pressures,  
19 that otherwise would tend to condense, can be studied. Moreover, the pulsed nozzle produces  
20 much less gas flow, requiring lower pumping speeds while yielding rate coefficients that are in  
21 satisfactory agreement with continuous flow measurements, as demonstrated in a collaborative  
22 work between Leone and coworkers and I. W. M. Smith and coworkers.<sup>13,25</sup>  
23  
24  
25  
26  
27  
28  
29  
30  
31  
32  
33  
34  
35  
36  
37

38 Although numerous low temperature kinetic measurements of the  $C_2H$  radical with  $C_2$  (in this  
39 paper,  $C_n$  denotes a hydrocarbon species containing  $n$  carbon atoms) and  $C_3$  hydrocarbons<sup>30</sup> have  
40 been performed during the last decade as well as product branching studies,<sup>17</sup> there are, to our  
41 knowledge, only a few measurements of rate coefficients with molecules having longer carbon  
42 chain lengths ( $C_4$  and higher).<sup>38,39</sup> As pointed out by Sims and coworkers,<sup>38</sup> highly unsaturated  
43 hydrocarbon species with four and more carbon atoms tend to be very unstable compounds  
44 because, for example, diacetylene polymerizes easily at room temperature. At the same time, the  
45 absence of these reactions in photochemical models can lead to underestimates of reaction  
46 pathways that otherwise would be non-negligible.<sup>40</sup> Furthermore, the photolysis of larger  
47 molecules may be a source of smaller neutral and radical species.<sup>40</sup> Therefore, it is suggested that  
48 future photochemical models will require including reactions of species containing four or more  
49  
50  
51  
52  
53  
54  
55  
56  
57  
58  
59  
60

1  
2  
3 carbon atoms, hence taking into account the underlying contributions of higher molecular weight  
4 species for more accurate chemical descriptions of Titan's atmosphere in models.  
5  
6  
7

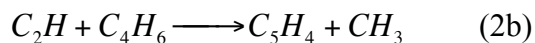
8 A recent study by Vuitton and coworkers<sup>41</sup> provides insight into the formation and distribution of  
9 benzene, a  $C_6$  hydrocarbon species, on Titan. The three-body propargyl recombination reaction  
10 (see Eq. 1) used in models<sup>42,43</sup> fails to predict the large mole fractions of benzene observed in the  
11 thermosphere on Titan.  
12  
13  
14



15  
16  
17  
18  
19  
20  
21 Indeed, three-body reactions are unlikely at low densities ( $\sim 10^{12} \text{ cm}^{-3}$  of  $N_2$  at an altitude of  $\sim 800$   
22 km).<sup>41</sup> Considering the time constants of key ion reactions,<sup>41</sup> the authors suggest that benzene in  
23 the ionosphere is likely produced by ion-molecule chemistry. The globally averaged column-  
24 integrated production rate of benzene in the ionosphere ( $\sim 10^7 \text{ cm}^{-2}\text{s}^{-1}$ ) is found to be of the same  
25 order of magnitude as the radical-neutral production rate ( $\sim 4 \times 10^6 \text{ cm}^{-2}\text{s}^{-1}$ ). The radical-neutral  
26 ( $C_2H + C_4H_6$ ) and radical-radical ( $C_2H_3 + C_4H_3$ ) reactions are identified as potential reactions to  
27 be included in models and the authors strongly emphasized that low temperature rate coefficients  
28 and product identification are required for these reactions. Conversely, in a recent combustion  
29 study, Hansen and coworkers<sup>44</sup> showed that  $C_6H_6$  is formed primarily through  $C_3H_3 + C_3H_3$  and *i*-  
30  $C_4H_5 + C_2H_2$ . In flames, the concentration of propargyl radicals is much higher and the formation  
31 of benzene *via* this pathway is more favorable. It is therefore of fundamental interest to explore  
32 the possible formation reactions of  $C_6$  molecules in the cold, low pressure and photochemically  
33 driven atmospheres of the outer planets, and especially Titan.  
34  
35  
36  
37  
38  
39  
40  
41  
42  
43  
44

45  
46 Carbon-containing radicals usually react with unsaturated hydrocarbon species where a short-  
47 lived intermediate<sup>45</sup> is formed and decomposes to give the substituted product, i.e. H-loss channel  
48 or  $CH_3$ -loss channel<sup>17</sup> (see Eqs. 2a and 2b). The reaction of  $C_2H$  with a  $C_4$  substituted alkyne, 1-  
49 butyne ( $C_4H_6$ ), is one such reaction with the possibility of forming cyclic  $C_6$  molecules, in  
50 particular benzene.  
51  
52  
53  
54





Indeed, in this study we have identified  $C_6H_6$  as one of the reaction products, corresponding to the H-loss channel according to Eq. 2a. Also, we have identified  $C_5H_4$  consistent with the  $CH_3$ -loss channel as indicated in Eq. 2b. However, in our study the formation of benzene is not observed. The product detection using Multiplexed Photoionization Mass Spectrometry (MPIMS) coupled to tunable VUV synchrotron radiation is intriguing, revealing the presence of cyclic isomers of  $C_6H_6$  other than benzene, as well as linear isomers. In this paper, we first report low temperature rate coefficient measurements for the reaction of the ethynyl radical with 1-butyne over the 74-295 K temperature range in a pulsed Laval nozzle using a chemiluminescence tracer method. The product detection and isomer identification are performed in a slow flow reactor using Multiplexed Photoionization Mass Spectrometry. Time-resolved Photoionization Efficiency (PIE) curves, i.e. the ion signal as a function of the synchrotron photon energy, for the two product channels are measured. The different product isomers appear as distinct thresholds and are identified according to their ionization energies and the shapes of their Franck-Condon profiles. The implications of these results for polyynes formation and their potential role for molecular weight growth chemistry in planetary atmospheres, especially on Titan, are also discussed.

## 2. Experiment

Two different apparatuses are used to study the reaction of the ethynyl radical ( $C_2H$ ) with 1-butyne ( $C_4H_6$ ). First, low temperature kinetic measurements are made in a pulsed Laval nozzle apparatus, followed by isomer-resolved product branching studies using a Multiplexed Photoionization Mass Spectrometer (MPIMS) coupled to tunable VUV synchrotron radiation at the Advanced Light Source at the Lawrence Berkeley National Laboratory. Experimental details such as error bars for the kinetics measurements, signal-to-noise ratio and data collection are also discussed. Calculations using the CBS-QB3 composite method<sup>46,47</sup> are performed to determine adiabatic ionization energies of  $C_5H_4$  and  $C_6H_6$  isomers relevant to this work. Photoionization energy curves are computed using the PESCAL program of Ervin.<sup>48,49</sup>

## 2.1. Low temperature Laval kinetics

The rate coefficients are measured in a pulsed Laval nozzle apparatus using laser photolysis and the chemiluminescence tracer method. A detailed description and schematic of the apparatus has been reported elsewhere.<sup>21</sup> In this paper, only the main features of the experiment will be presented. The experimental setup consists of a Laval nozzle mounted on a reservoir block under medium vacuum (0.1 – 1.0 Torr maintained by a Leybold Heraeus RuVac WS 1000 vacuum pump). Pulsed valves (solenoid Parker valve) are used to inject the gas mixture into the reservoir (1 cm<sup>3</sup> in volume) where the stagnation pressure is monitored by a pressure transducer (Omega PX170 series). The nozzle assembly is mounted on a movable yoke manually driven from outside the chamber. The nozzles used in this study have been characterized in detail.<sup>21</sup>

C<sub>2</sub>H radicals are created coaxially within the uniform supersonic expansion by pulsed laser photolysis of acetylene (C<sub>2</sub>H<sub>2</sub>) using an unfocused beam at 193 nm (Lambda Physik COMPex Pro 110 ArF). The diameter of the laser beam is limited by the throat of the Laval nozzle (1 cm in diameter). The laser energy is typically ~15 mJ/cm<sup>2</sup> after the divergent section of the nozzle. The concentration of C<sub>2</sub>H radicals inside the flow is monitored by the chemiluminescence tracer method (C<sub>2</sub>H + O<sub>2</sub> → CH (A<sup>2</sup>Δ) + CO<sub>2</sub>). The detection zone is situated ~10 cm downstream from the exit of the nozzle where light emitted perpendicular to the molecular beam propagation direction is filtered with a 430±10 nm band-pass filter and detected using a photomultiplier tube. The chemiluminescence signal is recorded using a multichannel scaler (model SR430) in a single photon-counting mode. A typical decay transient is obtained by accumulating ~12,000 photolysis laser pulses. The apparatus is run at a 10 Hz repetition rate. Synchronization of the various experimental components is achieved using a SRS DG535 Digital Delay Generator.

The N<sub>2</sub>, O<sub>2</sub> and C<sub>2</sub>H<sub>2</sub> gas flows are supplied directly from cylinders through stainless steel lines and controlled by individual calibrated mass flow controllers (MKS Mass-Flo Analog). The 1-butene cylinder is kept in a cold bath at 278 K to lower its vapor pressure, thus preventing condensation in the gas lines. The gases used in these measurements are as follows: the main carrier gas is N<sub>2</sub> (99.999%), C<sub>2</sub>H<sub>2</sub> (99.6%) is used as the radical precursor, O<sub>2</sub> (99.998%), 1-butene (98% Sigma Aldrich). The acetylene tank is equipped with an activated charcoal cartridge



1  
2  
3 filter to remove acetone, present in the tank as a stabilizing agent, prior to mixing in the main gas  
4  
5 flow.  
6  
7

## 8 **2.2. Photoionization Mass Spectrometry (PIMS)**

9  
10 The reaction products formed from the reaction of C<sub>2</sub>H with 1-butyne are measured in a slow  
11 flow tube reactor coupled to tunable vacuum ultraviolet (VUV) synchrotron radiation at the  
12 Advanced Light Source in Berkeley.<sup>50</sup> The Multiplexed Photoionization Mass Spectrometer  
13 building upon the general PIMS design of Slagle and Gutman,<sup>51</sup> has been described in previous  
14 studies<sup>17,50,52</sup> and only a brief overview will be given here. The instrument has benefitted from a  
15 recent major upgrade: the magnetic sector mass spectrometer described previously has been  
16 replaced by an orthogonal accelerated time-of-flight (OA-TOF) mass spectrometer with a  
17 superior mass resolution of ~2000. Briefly, the main He gas flow is seeded with the reactants: the  
18 C<sub>2</sub>H precursor and 1-butyne. All flows are controlled using calibrated mass flow controllers. The  
19 pressure inside the flow tube is maintained at 4 Torr (533.3 Pa) by adjusting the pumping speed  
20 of the Roots blower using a butterfly valve. At this pressure and room temperature, the total  
21 density inside the flow reactor is  $1.3 \times 10^{17} \text{ cm}^{-3}$ . The densities of the C<sub>2</sub>H precursor and 1-butyne  
22 are  $2.6 \times 10^{16} \text{ cm}^{-3}$  and  $5.0 \times 10^{14} \text{ cm}^{-3}$  respectively. The same excimer laser (Lambda Physik  
23 COMPex Pro 110 ArF) is used for photolysis but at a lower repetition rate (4 Hz). The measured  
24 energy per pulse at the exit of the tube is typically ~27 mJ/cm<sup>2</sup>. The unfocused 193 nm laser  
25 beam propagates collinearly down the reactor, a 62 cm long quartz tube with a 1.05 cm inner  
26 diameter, generating an initial uniform concentration of C<sub>2</sub>H radicals along the tube. The flow  
27 velocity inside the reactor is kept constant ~4 m/s. These conditions ensure the photolysis of a  
28 fresh gas mixture for each laser pulse. Neutral species escape from a 650 μm diameter pinhole on  
29 the side of the quartz tube forming an effusive beam that is skimmed by a 0.15 cm diameter  
30 skimmer and crossed by tunable VUV synchrotron radiation (8.1-10.1 eV). All ions are  
31 monitored simultaneously using an orthogonal accelerated time-of-flight mass spectrometer  
32 equipped with a micro-channel plate detector. Time-dependent, multiplexed mass spectra are  
33 recorded as a function of the synchrotron photon energy to obtain Photoionization Efficiency  
34 curves (PIE). Different structural isomers of the same chemical formula generally have PIE  
35 curves that exhibit unique ionization thresholds (ionization energies), shapes (determined by the  
36  
37  
38  
39  
40  
41  
42  
43  
44  
45  
46  
47  
48  
49  
50  
51  
52  
53  
54  
55  
56  
57  
58  
59  
60

1  
2  
3 Franck-Condon overlap between neutral and cation) and absolute intensities (determined by the  
4 electronic transition dipole moment).  
5  
6

7  
8 For the product detection study, the data were taken using 3,3,3-trifluoropropyne ( $\text{CF}_3\text{C}_2\text{H}$ ) as the  
9 radical precursor source rather than acetylene ( $\text{C}_2\text{H}_2$ ) as was used in the Laval nozzle  
10 measurements. This choice was made in order to optimize the signal-to-noise ratio of the two  
11 product channels in the mass spectrometer for the title reaction. Indeed, previous experiments<sup>17</sup>  
12 have shown that  $\text{CF}_3\text{C}_2\text{H}$  is a factor of two more efficient than acetylene in producing  $\text{C}_2\text{H}$   
13 radicals at 193 nm. To ensure a linear response of the ion detector, the average ion count rates are  
14 limited to 25 kHz. The photolysis of 1-butyne at 193 nm produces photoproducts (mainly  
15 propargyl radicals,  $\text{C}_3\text{H}_3$ , with an IE of 8.67 eV<sup>53</sup> and methyl radicals,  $\text{CH}_3$ ) that are additional  
16 species that contribute to the total number of ions arriving on the detector. This unwanted  
17 photolysis requires using a minimal amount of 193 nm laser fluence in the flow tube. Therefore  
18 to avoid detector saturation and to enhance the product ion signals,  $\text{CF}_3\text{C}_2\text{H}$  was used as the  
19 radical precursor source. Also, above 10.1 eV, the excess reactant, 1-butyne (with an IE of 10.20  
20 eV),<sup>54</sup> in the flow will ionize, increasing the total ion count rate above the acceptable range. With  
21 the present experimental apparatus, data could not be obtained above the ionization energy of 1-  
22 butyne.  
23  
24  
25  
26  
27  
28  
29  
30  
31  
32  
33  
34  
35  
36

37 The purities of the different gasses are as follows: He, 99.9999%;  $\text{CF}_3\text{C}_2\text{H}$ , 99%;  $\text{C}_2\text{H}_2$ , 99.6%  
38 and 1-butyne, 98%. Acetone is removed from the acetylene using a charcoal filter as described in  
39 the previous section.  
40  
41  
42  
43

### 44 **2.3. Computational methods**

45  
46 Adiabatic ionization energies were calculated using the CBS-QB3 composite method of  
47 Petersson and coworkers.<sup>46,47</sup> Simulated photoionization efficiency curves, based on the  
48 geometries, frequencies, and normal coordinates from the CBS-QB3 calculations, were computed  
49 using the PESCAL program of Ervin,<sup>48,49</sup> including full Duschinsky rotation for all totally  
50 symmetric modes. The resulting PIE spectra were convolved with a 30 meV FWHM Gaussian  
51 function to account for the instrumental resolution. Only the ground electronic states of the  
52 cations were included in the calculations, and no attempt was made to predict or model  
53  
54  
55  
56  
57  
58  
59  
60

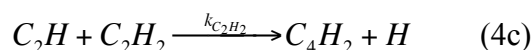
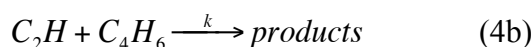
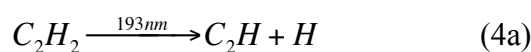
1  
2  
3 autoionizing resonances. The calculated ionization energies for the C<sub>6</sub>H<sub>6</sub> isomers reported in  
4 Table 1 are generally within 0.1 eV of the reported experimental values. Our calculated values for  
5 the C<sub>5</sub>H<sub>4</sub> isomers listed in Table 2 are also in good agreement with reported literature values.  
6  
7  
8  
9

### 10 11 12 **3. Results**

13  
14 In this section, the low temperature kinetic measurements will be presented first, followed by the  
15 identification of the product channels, identification of the individual isomers and product  
16 branching ratios for the reaction in the slow flow tube reactor coupled to VUV synchrotron  
17 radiation detection.  
18  
19  
20

#### 21 22 **3.1. Low temperature rate coefficients**

23  
24 Since the measured percentage depletion for acetylene, as detailed in Section 3.2.1 below, by the  
25 photolysis laser at 193 nm (see Eq. 4a) is only 0.5 %, it can be assumed that the concentration of  
26 the ethynyl radicals, [C<sub>2</sub>H], is much lower than the concentrations of the molecular species, i.e.  
27 1-butyne, acetylene and oxygen. Therefore, C<sub>2</sub>H radicals are likely to be consumed in the radical-  
28 molecule reactions as shown in Eqs. 4b to 4d rather than radical-radical reactions. A constant  
29 amount of O<sub>2</sub> is added in the flow in order to monitor the decay of the C<sub>2</sub>H radical concentration  
30 as explained below.  
31  
32  
33  
34  
35  
36  
37



42  
43  
44  
45  
46  
47  
48 From the reaction scheme outlined above the rate of change of the concentration of C<sub>2</sub>H radicals  
49 can be expressed as,  
50  
51  
52

$$53 \quad -\frac{d[C_2H]}{dt} = [C_2H](k_{C_2H_2}[C_2H_2] + k_{O_2}[O_2] + k[C_4H_6]) \quad (5a)$$

$$54 \quad = k_{obs}[C_2H]$$

Integrating Eq. 5a with respect to time yields Eq. 5b:

$$[C_2H] = [C_2H]_0 \exp[-k_{obs}t] \quad (5b)$$

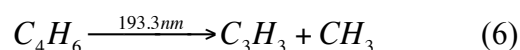
where  $k_{C_2H_2}$  and  $k_{O_2}$  are the rate constants for the reaction of the ethynyl radical with acetylene and oxygen respectively.  $[C_2H]_0$  is the initial concentration of ethynyl radicals. The rate constant for the reaction of  $C_2H$  with 1-butyne,  $k$ , is determined by plotting the pseudo first-order rate constants,  $k_{obs}$ , as a function of the concentration of 1-butyne,  $[C_4H_6]$ , while keeping the concentrations of oxygen and acetylene constant. Chemiluminescence from the electronically excited CH ( $A^2\Delta$ ) state (see Eq. 4d) at 431.22 nm<sup>55</sup> is used to monitor the time evolution of the  $C_2H$  radicals in the Laval flow. Because the radiative lifetime for free CH ( $A^2\Delta$ ) radicals (440( $\pm$ 20) ns)<sup>56</sup> is much shorter than the reaction timescale of the ethynyl radicals, a quasi-steady-state approximation can be made for the concentration of CH ( $A^2\Delta$ ). Therefore, it can be assumed that the chemiluminescence emission is directly proportional to the concentration of  $C_2H$  radicals present in the collimated supersonic expansion.

Figure 1 shows a typical decay trace of the chemiluminescence signal as a function of time. The experimental data can be fit by a single exponential function and confirms the pseudo-first-order approximation made in Eqs. 5a and 5b. The time interval for the fit for each decay curve is  $15 < t < 200 \mu s$ , hence avoiding interference from scattered light and emission produced by the 193 nm laser pulse. This initial 15  $\mu s$  time delay also allows for the quenching of excited  $C_2H$  radicals by nitrogen molecules.<sup>57</sup> As reported previously in the study of the reaction of  $C_2H$  with benzene,<sup>16</sup> the typical quenching time of excited ethynyl radicals in the flow is less than 1  $\mu s$ .

The kinetic measurements are repeated for different concentrations of 1-butyne while keeping the concentrations of acetylene and oxygen constant. As shown in Figure 2, the plot of  $k_{obs}$  as a function of the concentration of 1-butyne is fit well by a straight line, whose slope is the rate constant,  $k$ , for the  $C_2H + 1$ -butyne reaction. This procedure is repeated using different Laval nozzles to examine the temperature dependence of the rate coefficient. At each temperature,  $k_{obs}$  is typically measured for nine to twelve different 1-butyne densities. The error bars for  $k_{obs}$  are

determined to be  $\pm 2\sigma$  of the single exponential fits. The accumulated uncertainties for the concentrations of 1-butyne (i.e. 0.5% depletion by the 193 nm laser and 1% error of the actual flow controller) are not shown in Figure 2. The values of the rate coefficients as a function of temperature are summarized in Table 3. The reported uncertainties for these measurements are 20 % and are discussed below.

At 193 nm and room temperature, the reported absorption cross-section for 1-butyne is significant ( $\sim 1 \times 10^{-18} \text{ cm}^2$ ).<sup>58</sup> As will be discussed in Section 3.2.1, our measurements indicate that the depletion in 1-butyne and acetylene are comparable, i.e.  $\sim 0.5$  %. Therefore, we can assume that the destruction of 1-butyne at 193 nm is negligible and does not affect the reported densities in the flow. No chemiluminescence signal at  $\sim 430$  nm is detected in the absence of the  $\text{C}_2\text{H}$  precursor, indicating that the  $\text{C}_2\text{H}$  photodissociation channel of 1-butyne is not significant. We identified  $\text{C}_3\text{H}_3$  and  $\text{CH}_3$  as the main photodissociation products of 1-butyne (see Eq. 6 and Section 3.2.1). So we conclude that acetylene photodissociation is the only source of  $\text{C}_2\text{H}$  radicals and that the single photon photodissociation of 1-butyne does not produce  $\text{C}_2\text{H}$  radicals in significant amounts so as to interfere with the reaction. Again, based on the percentage depletion measurements (radical species) and the actual densities of the reagents (molecular species) in the flow, the probability of radical-radical removal of  $\text{C}_2\text{H}$  is negligible compared to removal by radical + stable molecule reactions.



Decreasing the energy of the photolysis laser by a factor of 2 did not change the measured rate constants significantly. Fitting the present data to a temperature-dependent rate expression yields  $k = (2.4 \pm 0.5) \times 10^{-10} (\text{T}/295 \text{ K})^{-(0.04 \pm 0.03)} \text{ cm}^3 \text{ molecule}^{-1} \text{ s}^{-1}$ . However, as the temperature dependence is essentially negligible within the experimental uncertainties, we recommend for kinetic modeling that the average rate coefficient,  $k = 2.5 \times 10^{-10} \text{ cm}^3 \text{ molecule}^{-1} \text{ s}^{-1}$ , should be taken with a total uncertainty of 20%.

### 3.2. Tunable VUV isomer-specific product detection

The goal of product detection studies coupled with kinetics measurements is to identify and estimate branching ratios for the products of the reaction between the ethynyl radical with 1-butyne. In this respect, the reaction has been studied at 295 K and 533 Pa in the slow flow reactor using Multiplexed Photoionization Mass Spectrometry (MPIMS) with tunable VUV synchrotron radiation. Both time- and energy-resolved data have been collected as described in Section 2.2. Mass spectra as a function of the ionization energy are retrieved from the raw data by integrating over the whole reaction timescale of 80 ms. Note that mass spectra are also taken for 20 ms before the pulsing of the photolysis laser for background subtraction. In this way, identification by  $m/z$  ratio of all species involved in the reaction is obtained. Then, for a given mass, the evolution of the ion signal as a function of: (1) time, which reveals the chemical nature of the species, i.e. precursor, photolysis product, primary reaction product, or secondary reaction product, and (2) energy, which helps to determine and distinguish between different isomers, is analyzed. Indeed, the presence of different isomers with different ionization energies is revealed as different thresholds and shapes in the Photoionization Efficiency (PIE) curves.

Figure 3(a) shows a mass spectrum with the radical precursor and the reactant, 1-butyne, flowing in the buffer gas and Figure 3(b) shows a second mass spectrum with only 1-butyne, both acquired at 10.1 eV and integrated over 80 ms of reaction time, with the 193 nm photolysis laser and the same density of 1-butyne. Both mass spectra are background subtracted. Two mass peaks show a significant increase when the  $C_2H$  precursor is added:  $m/z = 64$  and  $m/z = 78$ . Given the measured rate coefficient for the reaction of  $C_2H$  with 1-butyne, the concentration of the reactants and the instrumental time resolution, it is not possible to measure the rise-time of these two products. However, the observed instrument-limited rise-time after the photolysis laser pulse and the fact that the ion signal for both masses remains constant at later times is consistent with the formation of a closed-shell, unreactive species. After careful inspection of the mass spectra in Figure 3, the following observations can be made:

1. The ion signal at  $m/z = 64$  ( $C_5H_4$ ) is almost entirely due to the simultaneous presence of  $C_2H$ , created by the photolysis laser, and 1-butyne. This result is consistent with the  $C_5H_4 + CH_3$  product channel for the title reaction.

- 1  
2  
3 2. The ion signal at  $m/z = 78$  ( $C_6H_6$ ) shows a significant enhancement (by a factor of  $\sim 6$ )  
4 when the radical precursor is added to the flow. This result is consistent with the  $C_6H_6 +$   
5 H product channel for the title reaction. But, it is noted that there is some background  
6 contribution to the  $m/z = 78$  ion signal in the absence of the  $C_2H$  radical precursor.  
7  
8  
9

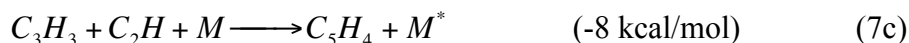
10  
11 Before analyzing these two ion signals, it is important to identify any side reactions that might  
12 interfere with the two product channels (see Section 3.2.1). As mentioned in Section 3.1, 1-  
13 butyne has a significant photodissociation cross-section at 193 nm, giving rise to additional  
14 radical species that can react with the reagents in the flow. In order to evaluate the contribution of  
15 these photodissociation products and extract the true signals for the title reaction, two separate  
16 sets of data, with the same concentration of 1-butyne in the flow, were collected (with and  
17 without the radical precursor). As seen in Figure 3(b), the contribution of 1-butyne  
18 photodissociation products to  $m/z = 64$  ion signal is negligible, showing that  $C_5H_4$  is indeed the  
19 product of the  $CH_3$ -loss channel for the title reaction. The PIE curve is analyzed in Section 3.2.2.  
20 However, the side reactions that produce  $m/z = 78$  ion signal are not negligible. Therefore, we  
21 extracted from the two sets of data a PIE curve for  $m/z = 78$  ions with ( $\blacklozenge$ ) and without ( $\otimes$ ) the  
22 radical precursor (see Figure 4 and caption for details). In this way, the increase in the ion signal,  
23 i.e. ( $\blacklozenge$ ) minus ( $\otimes$ ), is the contribution of products from the title reaction products to the  $m/z = 78$   
24 ion signal. The result is a PIE curve for the  $C_6H_6$  product channel, which is analyzed in Section  
25 3.2.3. Estimates of branching ratios are also derived for each product channel. Note that complete  
26 data sets in our experiment are limited to VUV photon energies between 8.2 and 10.1 eV due to  
27 experimental limitations as detailed in Section 2.2.  
28  
29  
30  
31  
32  
33  
34  
35  
36  
37  
38  
39  
40  
41  
42

### 43 **3.2.1. Photodissociation and photoproducts of reactants at 193 nm**

44  
45  
46 Figure 5 shows the photo-depletion measurements of (a) 1-butyne, (b) acetylene and (c) 3,3,3-  
47 trifluoropropyne recorded at 193 nm. These experiments have been done in order to quantify the  
48 photo-depletion of 1-butyne by the laser and to choose between acetylene and 3,3,3-  
49 trifluoropropyne for the  $C_2H$  precursor. Each data set is fit to a step function after the pulsing of  
50 the laser at 20 ms. The average laser energy is  $\sim 27$  mJ/pulse in all experiments and the measured  
51 percentage depletion as well as the composition of the gas mixtures are reported in Table 4. From  
52 these measurements, it can be noted that the photodepletion of 1-butyne and acetylene are  
53  
54  
55  
56  
57  
58  
59  
60

comparable, i.e. 0.45% and 0.47% respectively. As expected,<sup>59</sup> the photodissociation of 3,3,3-trifluoropropyne is more efficient by a factor of 2 (0.83%) compared to acetylene. In addition to the high yield of C<sub>2</sub>H radicals, the photolysis of CF<sub>3</sub>C<sub>2</sub>H leaves behind less reactive CF<sub>3</sub> radicals compared to H-atoms from acetylene. We have used 3,3,3-trifluoropropyne as the C<sub>2</sub>H radical precursor in order to optimize the signal for the two product channels because it allows us to increase the concentration of ethynyl radicals while keeping the 193 nm laser energy low enough to minimize 1-butyne photodissociation.

As mentioned in the previous section, 1-butyne has a significant photodissociation cross-section at 193 nm. It is most likely that the photoproducts are radical species that can further react with 1-butyne to yield stable hydrocarbons. These products can interfere with the product channels of the title reaction. Quantifying the contribution of these photodissociation products of the alkyne to the ion signals is therefore crucial in our experiment for accurate isomer-specific product detection. We have identified methyl (CH<sub>3</sub>, IE = 9.843 eV)<sup>60</sup> and propargyl (C<sub>3</sub>H<sub>3</sub>, IE = 8.67 eV)<sup>53</sup> as the two main radical species formed from the 193 nm photolysis of 1-butyne (not shown on mass spectra of Figure 3). CH<sub>3</sub> radicals can react with C<sub>4</sub>H<sub>6</sub> or CF<sub>3</sub>C<sub>2</sub>H molecules in the flow. However, it is unlikely that the products of the reaction will contribute to the ion signal at either m/z = 64 (C<sub>5</sub>H<sub>4</sub>) or 78 (C<sub>6</sub>H<sub>6</sub>). On the other hand, C<sub>3</sub>H<sub>3</sub> radicals could react with C<sub>4</sub>H<sub>6</sub> to produce C<sub>6</sub>H<sub>6</sub> (e.g. benzene) by losing a CH<sub>3</sub> radical according to Eq. 7a. The formation of C<sub>5</sub>H<sub>4</sub> (e.g. methylidyneacetylene) is found to be endothermic (Eq. 7b) and therefore not favorable. C<sub>3</sub>H<sub>3</sub> radicals could also react with CF<sub>3</sub>C<sub>2</sub>H to produce C<sub>5</sub>H<sub>4</sub> by losing a CF<sub>3</sub> radical.



However, reactions of propargyl with closed-shell molecules are relatively slow. On the other hand, recombination of two propargyl radicals could be a source of C<sub>6</sub>H<sub>6</sub> (Eq. 1). Similarly, C<sub>3</sub>H<sub>3</sub> + C<sub>2</sub>H could be a source of C<sub>5</sub>H<sub>4</sub> as shown in Eq. 7c, and it is unlikely that C<sub>2</sub>H + C<sub>2</sub>H will contribute to the ion signal at either m/z = 64 (C<sub>5</sub>H<sub>4</sub>) or 78 (C<sub>6</sub>H<sub>6</sub>). At the pressure of the present experiments (533 Pa), it is expected that stabilization dominates the propargyl + propargyl



1  
2  
3 reaction, with only about  $10^{-3}$  branching to phenyl + H.<sup>61</sup> Based on these considerations, we  
4 identify  $C_3H_3 + C_3H_3$  as the main side reaction contributing to the  $m/z = 78$  ion signal for pure 1-  
5 butyne photolysis. By flowing only the  $C_2H$  precursor in the buffer gas, we verified that no  
6 contribution of trifluoropropyne photoproducts to the two mass channels of interest was  
7 observed.  
8  
9

10  
11  
12  
13  
14 Figure 4 shows the PIE curves with and without the  $C_2H$  precursor for  $m/z = 78$  ion signal.  
15 Assuming that the main interference in the  $m/z = 78$  ion signal is the product of  $C_3H_3 + C_3H_3$  (Eq.  
16 1) and that  $C_6H_6$  is one product of the  $C_2H + 1$ -butyne reaction as shown in Eq. 4b and discussed  
17 above, we can subtract the  $m/z = 78$  ion signal resulting from propargyl recombination obtained  
18 without  $C_2H$  radicals present from the total ion signal for  $m/z = 78$  when  $C_2H$  radicals are  
19 present. This process yields the PIE curve for the title reaction, which is shown in Figure 6. For  
20  $m/z = 64$  ( $C_5H_4$ ), the PIE curve is shown in Figure 7. In the sections to follow, these two PIE  
21 curves are analyzed and estimates of branching ratios are derived for the  $C_5H_4$  and  $C_6H_6$  product  
22 channels.  
23  
24  
25  
26  
27  
28  
29

### 31 **3.2.2. $C_5H_4$ from the reaction of the ethynyl radical with 1-butyne**

32  
33

34 Figure 7 shows the PIE curve for the  $C_5H_4$  mass channel for the reaction of the ethynyl radical  
35 with 1-butyne. In our analysis of the observed PIE curve below, literature and calculated values  
36 of the ionization energies of the  $C_5H_4$  isomers are taken from the work of Goulay and  
37 coworkers<sup>17</sup> and Hansen and coworkers.<sup>62</sup> Because the absolute photoionization cross sections  
38 are not available for all of the  $C_5H_4$  isomers, we have used the single point estimates of  
39 photoionization cross sections already reported.<sup>17</sup> Hansen and coworkers<sup>62</sup> performed Franck-  
40 Condon simulations for ethynylallene ( $CH_2CCHCCH$ ), methylidyneacetylene and 1,4-pentadiyne in  
41 their study of  $C_5H_x$  isomers<sup>62</sup> for an assumed temperature of 300 K. The simulated  
42 photoionization efficiency curves are in very good agreement with their experimental data for the  
43  $C_5H_4$  isomers. In the absence of any reference data for these isomers, these simulated curves are  
44 used to fit our experimental data.  
45  
46  
47  
48  
49  
50  
51  
52  
53

54  
55 The observed PIE curve shown in Figure 7 can be fit between 8.1 and 9.9 eV by a weighted sum  
56 of Franck-Condon based simulations for the two most stable isomers of  $C_5H_4$ , i.e. ethynylallene  
57  
58  
59  
60

1  
2  
3 and methyldiacetylene. Since no threshold in the ion signal is observed at 8.67 eV, we conclude  
4 that the 1,2,3,4-pentatetraene isomer is not produced by the reaction. The first sharp rise in the  
5 ion signal at 9.15 eV is attributed to the presence of ethynylallene. The only reported adiabatic  
6 ionization energy for this isomer is 9.22 eV using QCISD(T) calculations,<sup>62</sup> in good agreement  
7 with our calculated value of 9.20 eV. The solid black line in Figure 7(a) indicates the fit including  
8 only the contribution of the CH<sub>2</sub>CCHCCH isomer. Note that the calculated photoionization  
9 efficiency curve increases slowly above 9.25 eV with a step around 9.5 eV,<sup>62</sup> almost coinciding  
10 with the next threshold in the ion signal. However, the fit assuming only ethynylallene  
11 contributes to the PIE curve between 8.1 and 9.9 eV is fairly poor, which suggests the presence of  
12 an additional isomer. It follows that the threshold at 9.5 eV is most certainly due to the presence  
13 of methyldiacetylene. Moreover, there is a good agreement between the simulated PIE curve and  
14 the actual experimental data, as seen in Figure 7(b), when the contribution from  
15 methyldiacetylene is taken into account in the overall fit up to 9.9 eV.  
16  
17  
18  
19  
20  
21  
22  
23  
24  
25  
26  
27

28 The observed signal as a function of energy,  $S(E)$ , is proportional to the sum of the individual  
29 photoionization cross sections,  $\sigma_i(E)$ , weighted by the mole fraction of each C<sub>5</sub>H<sub>4</sub> isomer,  $X_i$ , as  
30 indicated in Eq. 8. Reliable estimates for the photoionization cross sections can be obtained as  
31 described<sup>17</sup> using a semi-empirical model by Bobeldijk and coworkers.<sup>63</sup> With the reported  
32 values,<sup>17</sup> we can estimate a ratio for ethynylallene/methyldiacetylene of approximately 4:1 for the  
33 reaction of the ethynyl radical with 1-butyne.  
34  
35  
36  
37  
38  
39  
40

$$41 \quad S(E) \propto \sigma_{total}(E) = \sum_{i=1}^m \sigma_i(E) X_i \quad (8)$$

42  
43  
44  
45

46 Due to experimental limitations as described in Section 2.2, a complete set of data above  
47 10.125 eV could not be obtained. Therefore, in our experiment we cannot probe the presence or  
48 absence of 1,4-pentadiyne (IE = 10.27 eV).<sup>54</sup> The gray dashed line in Figure 7(b) represents the  
49 calculated PIE curve of 1,4-pentadiyne. The residual of the fit with ethynylallene and  
50 methyldiacetylene in Figure 7 suggests the presence of another ionization threshold near 9.95 eV.  
51 However, as seen by Goulay and coworkers<sup>17</sup> in the reaction of C<sub>2</sub>H + propyne, the ion signal for  
52  $m/z = 64$  should follow a slight linear increase as a function of photon energy above 9.8 eV when  
53  
54  
55  
56  
57  
58  
59  
60

1  
2  
3 only ethynylallene and methyldiacetylene are present. This would suggest that the observed  
4 threshold in our experiment might be due to the presence of another  $C_5H_4$  isomer. Nevertheless,  
5 based on the molecular structure of methyldiacetylene (IE = 9.47 eV) and 1,4-pentadiyne (IE =  
6 10.27 eV), i.e. both molecules have two triple bonds, compared with ethynylallene (with a lower  
7 IE = 9.20 eV), which has two double bonds and a single triple bond, it is hard to propose a  
8 rational structure of a linear  $C_5H_4$  isomer that could possibly have an ionization energy around 10  
9 eV. Also, this threshold feature could be explained by dissociative ionization of a heavier  
10 molecule or the presence of an electronically excited state of  $C_5H_4^+$ . Again, in the absence of a  
11 complete set of data at higher photon energies, we can only quantify the isomeric distribution of  
12 methyldiacetylene and ethynylallene.  
13  
14  
15  
16  
17  
18  
19  
20  
21  
22

23 The fit of the PIE curve, indicated as a thick black line is shown in Figure 7(b), is the sum of the  
24 individual contributions (FC simulations) of ethynylallene (dashed line) and methyldiacetylene  
25 (dotted line). The PIE curve is normalized to the total estimated cross section at 9.8 eV of an  
26 average mixture of 82( $\pm$ 15)% of ethynylallene and 18( $\pm$ 15)% of methyldiacetylene using  
27 estimated photoionization cross sections reported in Table 5.  
28  
29  
30  
31

### 32 **3.2.3. $C_6H_6$ from the reaction of the ethynyl radical with 1-butyne**

33  
34  
35

36 Figure 6 shows the photoionization efficiency curve for  $m/z = 78$  ( $C_6H_6$ ) mass channel, from the  
37 reaction of the  $C_2H$  radical and 1-butyne. Relative photoionization efficiency curves are used  
38 when available for some of the  $C_6H_6$  isomers considered herein.<sup>64</sup> The 8.2-9.1 eV range exhibits a  
39 very slow monotonic rise in the ion signal. At 8.36 eV a first threshold is observed,  
40 corresponding to the ionization energy of the cyclic 5-membered  $C_6H_6$  isomer, fulvene.  
41 Furthermore, the onset of the signal can be replicated by its relative PIE curve.<sup>64</sup> A second  
42 threshold is identified at 8.8 eV. In this portion of the PIE curve, a single contribution by fulvene  
43 cannot account for the observed signal as shown in Figure 6(b). This second onset corresponds to  
44 the ionization energy of 3,4-dimethylenecyclobut-1-ene (DMCB), a 4-membered cyclic isomer of  
45  $C_6H_6$ . A good fit is obtained with a weighted sum including the relative PIE curves for fulvene  
46 and DMCB, further confirming the presence of the latter. Using estimated values<sup>44</sup> for the  
47 photoionization absorption cross sections of these two species (see Table 6), these isomers are  
48 formed in an approximate ratio of 1:2.  
49  
50  
51  
52  
53  
54  
55  
56  
57  
58  
59  
60

1  
2  
3  
4  
5 The residual of the fit including fulvene and DMCB (thick black line in Figure 6(b)) indicates a  
6 small feature between 8.9-9.4 eV followed by a sharp increase in the photoionization signal  
7 around 9.4 eV. In this energy range, there are four possible C<sub>6</sub>H<sub>6</sub> isomers: 2-ethynyl-1,3-  
8 butadiene (IE = 8.95 eV), 3,4-hexadiene-1-yne (IE = 8.99 eV), benzene (IE = 9.24 eV)<sup>65</sup> and 1,3-  
9 hexadiyne (IE = 9.41 eV<sup>66</sup>). The relative PIE curve of benzene is well known<sup>64</sup> while those of 2-  
10 ethynyl-1,3-butadiene, 3,4-hexadiene-1-yne and 1,3-hexadiyne have been computed as discussed  
11 in Section 2.3. Benzene has a very distinctive onset and characteristic PIE curve<sup>64</sup> shape that does  
12 not seem to match with the feature observed around 9.3 eV. Since the small onset occurs before  
13 the well-defined ionization potential of benzene, the small feature is more likely related to 2-  
14 ethynyl-1,3-butadiene and 3,4-hexadiene-1-yne. Indeed, a good fit (solid black line) of the  
15 experimental data is obtained up to 9.35 eV when a weighted contribution of 2-ethynyl-1,3-  
16 butadiene (dotted line) and 3,4-hexadiene-1-yne (dashed line) is included as shown in Figure  
17 6(c). Note that the calculated IE of 1,3-hexadiene-5-yne (8.63 eV) is found to be 0.6 eV lower  
18 than the reported experimental value (9.3 eV), which is an estimated value from electron impact  
19 measurements.<sup>66</sup> No threshold in the ion signal is observed around 8.6 eV indicating that 1,3-  
20 hexadiene-5-yne is not produced in significant amounts. Although it is therefore difficult to  
21 firmly quantify benzene in our experiment, it is probably not produced in significant quantities.  
22  
23  
24  
25  
26  
27  
28  
29  
30  
31  
32  
33  
34  
35  
36

37 It is likely that the next threshold observed at 9.4 eV is due to the linear C<sub>6</sub>H<sub>6</sub> isomer, 1,3-  
38 hexadiyne. Additional thresholds above 9.4 eV are not observed, indicating that 1,4-hexadiyne  
39 and 1,5-hexadiyne are also negligible reaction products. The fit of the PIE curve, indicated as a  
40 thick black line, is the sum of the individual contributions (FC simulations) of fulvene, DMCB,  
41 2-ethynyl-1,3-butadiene, 3,4-hexadiene-1-yne and 1,3-hexadiyne. The PIE curve is normalized to  
42 the total estimated cross section of an average mixture of 18% of fulvene, 32% of DMCB, 8% of  
43 2-ethynyl-1,3-butadiene, 28% of 3,4-hexadiene-1-yne and 14% of 1,3-hexadiyne using the  
44 estimated photoionization cross sections at 10 eV (see Table 6). Within experimental  
45 uncertainties, an upper limit of 10 % is estimated for benzene production.  
46  
47  
48  
49  
50  
51  
52  
53  
54  
55  
56  
57  
58  
59  
60

## 4. Discussion

In this paper, we present the only experimental work reporting both low temperature kinetics and room temperature product detection of the ethynyl radical ( $C_2H$ ) with a  $C_4$  molecule, 1-butyne. The rate coefficient measurements, within experimental uncertainty, exhibit almost no temperature dependence in the 74-295 K range as shown in Figure 8. Using photoionization mass spectrometry coupled to tunable VUV synchrotron radiation, we have direct information about the product channels involved (4 Torr, 295K) and we have been able to determine and distinguish between the different isomers present. We discuss below the probable mechanism for the reaction of the  $C_2H$  radical and 1-butyne and the possible implications for the photochemistry of the outerplanets, especially the Saturnian moon Titan.

### 4.1. Temperature dependence and reaction mechanism

It is worthwhile to compare the measured rate coefficients of the reaction of the  $C_2H$  radical with 1-butyne (or ethylacetylene) with the smaller alkynes, i.e. acetylene ( $C_2H_2$ ) and propyne (or methylacetylene,  $C_3H_4$ ). Figure 8 shows a plot of the rate constants for the title reaction as a function of temperature along with analogous measurements for acetylene and propyne obtained in a collaborative work between Leone and coworkers and Sims and coworkers.<sup>13,25</sup> As pointed out by Sims and coworkers<sup>13</sup>, the results obtained independently using a pulsed and a continuous Laval nozzle are in satisfactory agreement. Moreover, a general rule of thumb is derived by taking the measured rate coefficient for acetylene ( $k_{C_2H_2} = 1.9 \times 10^{-10} \text{ cm}^3 \text{ molecule}^{-1} \text{ s}^{-1}$  at  $T \approx 50 \text{ K}$ ) and its ionization energy of 11.4 eV as a reference to estimate low temperature rate coefficients of  $C_3$  and  $C_4$  alkenes and alkynes as a function of their ionization energies. Using this correlation, it is expected that the rate constant should increase with molecular mass (or decreasing ionization energy) for the corresponding alkenes, alkynes, dienes and diynes. As shown in Figure 8, the measured rate coefficient with  $C_4H_6$  ( $k = 2.6 \times 10^{-10} \text{ cm}^3 \text{ molecule}^{-1} \text{ s}^{-1}$  at  $T \approx 74 \text{ K}$ ) is higher than  $C_2H_2$  but comparable with  $C_3H_4$  and is therefore in agreement with the expected trend. It should be noted that in the temperature range 70-100 K, the reaction with the  $C_2H$  radical is rapid and close to the collision-determined limit. Our data is also consistent with the measured rate coefficients of the  $C_2H$  with 1,3-butadiene reaction.<sup>39</sup> Indeed, our rate constant is slightly lower

1  
2  
3 than the  $C_4$  diene ( $k_{C_2H} = 2.9 \times 10^{-10} \text{ cm}^3 \text{ molecule}^{-1} \text{ s}^{-1}$  at  $T \approx 104 \text{ K}$ ), which is in agreement with  
4  
5 the lower ionization energy of  $9.072 \text{ eV}^{67}$  for 1,3-butadiene. No measurements of rate  
6  
7 coefficients for the reactions of  $C_2H$  and the two other linear  $C_4H_6$  isomers, i.e. 1,2-butadiene (IE  
8  
9 =  $9.03 \text{ eV}^{68}$ ) and 2-butyne (IE =  $9.59 \text{ eV}^{54}$ ) are available. However, our results combined with  
10  
11 previous studies<sup>39</sup> suggest that the rate coefficients for these reactions should be comparable. The  
12  
13 reaction of the  $C_2H$  radical with linear  $C_4H_6$  isomers is most probably barrierless, showing almost  
14  
15 no temperature dependence and a rate coefficient can be estimated to be in the range  $(2.5\text{-}3.0) \times$   
16  
17  $10^{-10} \text{ cm}^3 \text{ molecule}^{-1} \text{ s}^{-1}$ .

18  
19  
20 Before considering the possible mechanism for the reaction, it is useful to compare the energetics  
21  
22 of propargyl recombination,<sup>61</sup> which has been identified as a benzene formation pathway in fuel-  
23  
24 rich flames.<sup>44</sup> Figure 9 shows the heats of reaction ( $\Delta H_r^\circ$  in kcal/mol) in which the three most  
25  
26 stable  $C_6H_6$  isomers, i.e. DMCB, fulvene and benzene, are produced. The three-body  
27  
28 recombination of two propargyl radicals leading to  $C_6H_6$  isomers is more exothermic ( $\sim 38$   
29  
30 kcal/mol) compared to the formation of the same isomers through the H-loss channel of  $C_2H + 1$ -  
31  
32 butyne reaction. In the latter case, the  $C_6H_6$  products are left with less internal energy and as a  
33  
34 consequence further isomerizations on the  $C_6H_6$  potential energy surface to form more stable  
35  
36 isomeric structures, e.g. DMCB to fulvene or fulvene to benzene, are probably less facile. In fact,  
37  
38 most of the isomerization transition states calculated by Miller and Klippenstein are predicted to  
39  
40 be energetically inaccessible for the  $C_6H_6$  product of the  $C_2H + 1$ -butyne reaction, so the  
41  
42 isomerization steps that determine the product distribution most likely take place on the  $C_6H_7$   
43  
44 surface. The heats of formation of methyldiacetylene ( $-39 \text{ kcal/mol}$ ), diacetylene ( $-36 \text{ kcal/mol}$ )  
45  
46 and DMCB ( $-43 \text{ kcal/mol}$ ) for the title reaction are all comparable. Because methyldiacetylene  
47  
48 and DMCB are detected in the reaction at room temperature, the  $C_2H_5$ -loss channel to form  $C_4H_2$   
49  
50 (diacetylene) is presumably also accessible. However, the ionization energy of diacetylene,  $10.17$   
51  
52 eV, is too close to that of 1-butyne, and we cannot operate at high enough photon energies to  
53  
54 directly probe this channel in our experiment.

55  
56 Reactions of non-resonance-stabilized carbon-centered radicals with unsaturated hydrocarbons  
57  
58 are expected to proceed *via* an intermediate<sup>16,17,69</sup> formed with almost no activation energy.<sup>45</sup>  
59  
60 Subsequently, the short-lived intermediate decomposes to give the final products of the reaction

1  
2  
3 whose isomeric structure depends upon the energy available in the system. Within the  
4 temperature range 74-295 K and pressure range 0.1-1 Torr, the measured total rate coefficient for  
5 the reaction is almost constant, and close to the collision-determined limit as mentioned above.  
6 This behavior suggests that back dissociation of the intermediate is negligible. Also for the  
7 reaction between C<sub>2</sub>H and acetylene, as shown experimentally<sup>15,21,22</sup> and theoretically,<sup>15,70</sup> the  
8 entrance channel of the reaction is the attack of the  $\pi$  electrons by the radical to form an  
9 intermediate that in turn decomposes to give diacetylene as the final product, consistent with an  
10 addition-elimination reaction. The hydrogen abstraction mechanism whereby a H-atom is  
11 captured by the C<sub>2</sub>H radical to form acetylene is also thermodynamically feasible. In the case of  
12 C<sub>2</sub>H + C<sub>2</sub>H<sub>2</sub>, Ceursters and coworkers<sup>15</sup> calculated a barrier of  $\sim 40$ -45 kJmol<sup>-1</sup> for the direct H-  
13 abstraction while addition-elimination of C<sub>2</sub>H is essentially barrierless. The close to collision-  
14 determined limit rates of reaction indicate that addition-elimination predominates over  
15 abstraction in such reactions involving the C<sub>2</sub>H radical with hydrocarbons.<sup>17</sup>  
16  
17  
18  
19  
20  
21  
22  
23  
24  
25  
26  
27

28 By analogy to the study of Ceursters and coworkers,<sup>15</sup> it is expected that the C<sub>2</sub>H radical will add  
29 to the triple bond of the 1-butyne molecule. In principle, the C<sub>2</sub>H addition proceeds by the direct  
30 attack on either of the triply bonded carbon atoms, giving rise to an acyclic radical species.<sup>15</sup> In  
31 the reaction of C<sub>2</sub>H with acetylene, the cyclic three-membered and four-membered ring radicals  
32 are found to be far less stable compared to the open radical structure. Moreover, the three-  
33 membered ring radical can easily rearrange to the open form because both structures are  
34 separated by a barrier of 5.7 kcal/mol (24 kJ/mol).<sup>15</sup> A similar situation can be expected for the  
35 title reaction. The initially formed radical can isomerize prior to dissociation. Senosiain and  
36 Miller<sup>71</sup> have reported several stationary points of C<sub>6</sub>H<sub>7</sub> related to the addition of acetylene to *n*-  
37 and *i*-C<sub>4</sub>H<sub>5</sub> radicals. The intermediates in those reactions are not directly relevant to the present  
38 reaction, but because the C<sub>2</sub>H + 1-butyne asymptote lies higher in energy than many of the  
39 calculated isomerization transition states, that work is consistent with relatively facile  
40 isomerization of the initially formed C<sub>6</sub>H<sub>7</sub> adduct in the C<sub>2</sub>H + 1-butyne reaction.  
41  
42  
43  
44  
45  
46  
47  
48  
49  
50  
51  
52

53 Starting with the radical formed by the direct attack of the terminal acetylenic carbon atom by  
54 C<sub>2</sub>H (see Figure 10), four different pathways leading to stable products (C<sub>3</sub>H<sub>4</sub> and C<sub>6</sub>H<sub>6</sub> isomers)  
55 can be proposed. These pathways include three different direct  $\beta$  scission reactions to  
56  
57  
58  
59  
60

1  
2  
3 ethynylallene formation *via* CH<sub>3</sub>-loss or either 1,3-hexadiyne or 3,4-hexadien-1-yne *via* H-loss. A  
4  
5 1,3 H shift followed by a H-loss, through a  $\beta$  scission, could form another linear C<sub>6</sub>H<sub>6</sub> isomer,  
6  
7 1,3-hexadien-5-yne. The barrier to a 1,3 H shift should be substantial,<sup>72</sup> but may still lie beneath  
8  
9 the reactant energy.

10  
11  
12 Similarly, three different evolution pathways can be proposed in the case of C<sub>2</sub>H addition to the  
13  
14 central carbon atom in the triple bond (see Figure 11). First, direct C<sub>2</sub>H<sub>5</sub>-loss through a  $\beta$  scission  
15  
16 reaction can lead to diacetylene (C<sub>4</sub>H<sub>2</sub>). Second, a 1,4 H shift followed by  $\beta$  scission forms 2-  
17  
18 ethynyl-1,3-butadiene or cyclization to a five-membered ring radical, which eventually  
19  
20 decomposes to yield fulvene. Third, a 1,3 H shift followed by cyclization to form the four-  
21  
22 membered radical structure can ultimately decompose to give 3,4-dimethylenecyclobut-1-ene  
23  
24 through  $\beta$  scission.

25  
26  
27 Based on the proposed reaction pathways, the formation of C<sub>5</sub>H<sub>4</sub> isomers most probably results  
28  
29 from terminal addition of the C<sub>2</sub>H radical to 1-butyne (see Figure 10). As seen from the PIE  
30  
31 curve in Figure 7, the 4:1 ratio in favor of the ethynylallene suggests that the diene is formed  
32  
33 preferentially as opposed to methyldiacetylene in the reaction between C<sub>2</sub>H with 1-butyne. This  
34  
35 observation is consistent with the proposed mechanism where ethynylallene production is facile,  
36  
37 because it results from a direct CH<sub>3</sub>-loss through a  $\beta$  scission reaction of the adduct formed after  
38  
39 terminal addition. Ultimately, the branching ratio for isomerization to methyldiacetylene will  
40  
41 probably depend on the amount of internal energy left in ethynylallene after reaction. Moreover,  
42  
43 the geometries of the adducts shown in Figures Figure 10 and Figure 11 suggest that 1,4-  
44  
45 pentadiyne formation is more complex than formation of ethynylallene. It can be argued that the  
46  
47 rearrangement leading to its formation is probably unfavorable.

48  
49 As suggested by the branching ratios of 18( $\pm$ 5)% and 32( $\pm$ 8)% for fulvene and 3,4-  
50  
51 dimethylenecyclo-but-1-ene (DMCB) respectively, 4- and 5-membered ring species are produced  
52  
53 in comparable proportions to the linear C<sub>6</sub>H<sub>6</sub> isomers, i.e. 8( $\pm$ 5)% of 2-ethynyl-1,3-butadiene,  
54  
55 28( $\pm$ 8)% of 3,4-hexadiene-1-yne and 14( $\pm$ 5)% of 1,3-hexadiyne. At the present time, there is no  
56  
57 potential energy surface available for the reaction between the C<sub>2</sub>H radical and C<sub>4</sub>H<sub>6</sub>. However,  
58  
59 the related systems of *n*- and *i*-C<sub>4</sub>H<sub>5</sub> + acetylene<sup>71</sup> and the recombination of two propargyl  
60



1  
2  
3 radicals on a  $C_6H_6$  potential energy surface<sup>61</sup> provides some insight into possible isomerization  
4 pathways. The benzene molecule has the deepest well, on the  $C_6H_6$  surface, followed by fulvene  
5 and DMCB. Our measurements demonstrate that benzene is probably not formed in significant  
6 amounts by this reaction at room temperature, where an upper limit of 10 % is estimated. The  
7 isomerization of DMCB or fulvene down to benzene must traverse substantial barriers. For  
8 instance, in the calculated fulvene to benzene paths,<sup>61</sup> benzene is the lower of the two isomers by  
9 about 31 kcal/mol (130 kJ/mol). However, approximately 75 kcal/mol (~314 kJ/mol) is required  
10 to overcome the barrier to isomerization. The presence of fulvene and DMCB products  
11 demonstrates that cyclization occurs in the  $C_6H_6 + H$  channel but suggests that the energy  
12 remaining in the  $C_6H_6$  product is not enough to readily overcome the barrier to benzene  
13 formation. However, the isomerization on the  $C_6H_7$  surface may be more facile. Calculated  
14 transition states for the 1,5- and 1,3-H shifts from other  $C_6H_7$  isomers produced in the  $C_4H_5 +$   
15 acetylene reactions<sup>71</sup> lie near or below the energy of the  $C_2H + 1$ -butyne reactants. It seems likely  
16 that the isomeric product distributions are largely determined by the dynamics on the  $C_6H_7$   
17 surface. Although the total rate coefficient is found to be independent of temperature over the  
18 range studied, the product distributions could still be temperature dependent.  
19  
20  
21  
22  
23  
24  
25  
26  
27  
28  
29  
30  
31

## 32 **4.2. Implication for Titan's photochemistry**

33 Reactions of unsaturated  $C_2$  hydrocarbon radicals<sup>73</sup> with hydrocarbon species are considered to  
34 play a central role for the formation of carbon rich species (polyynes and PAHs) in the interstellar  
35 medium, exo-planets and in the cold, photochemically active atmosphere on Titan.<sup>6,74</sup> In the  
36 course of these reactions, eventually two more carbon atoms are incorporated, thereby enlarging  
37 the carbon chain in the molecule and contributing to the complex process of molecular weight  
38 growth. These reactions can proceed *via* multiple intermediates, leading to different product  
39 channels and the initial isomeric structure can play a crucial role as demonstrated in the study  
40 with  $C_3H_4$  isomers.<sup>17</sup> Moreover, this study of 1-butyne shows that at least two competing product  
41 channels (H-loss and  $CH_3$ -loss) are active and of almost equal importance. In the case of  
42 acetylene, the mechanism involves the initial addition of the  $C_2H$  group to the  $\pi$ -electron system  
43 followed by the elimination of a hydrogen atom to form the product, diacetylene ( $C_4H_2$ ). The  
44 measured rate constant is near the collision limit and increases as a function of the number of  
45 carbon atoms in the chain. In devising ever more elaborate models for Titan's atmosphere, low  
46  
47  
48  
49  
50  
51  
52  
53  
54  
55  
56  
57  
58  
59  
60

1  
2  
3 temperature rate coefficient data including  $C_4$  and longer chain hydrocarbons will be required. In  
4 this respect, the low temperature kinetic measurements for the title reaction, together with the  
5 previous study of 1,3-butadiene<sup>39</sup> in our group, indicate that the reactions with  $C_4H_6$  isomers can  
6 occur at rates close to the collision limit at temperatures relevant to Titan's atmosphere, i.e. on  
7 the order of  $(2.5-3.0) \times 10^{-10} \text{ cm}^3 \text{ molecule}^{-1} \text{ s}^{-1}$ .  
8  
9

10  
11  
12  
13  
14 In this work, we also estimated the product branching ratios for the reaction of the  $C_2H$  radical  
15 with 1-butyne at room temperature and 4 Torr (533 Pa). Special care needs to be taken because it  
16 is known that extrapolation of data to lower temperatures is often problematic. However, the low  
17 temperature kinetic measurements for the reaction of the ethynyl radical with 1-butyne do not  
18 show any temperature dependence in the range 74-295 K. This behavior is indicative of a  
19 reaction without an activation barrier. In this case, the rate-limiting step of the reaction is the  
20 addition of the  $C_2H$  radical to the triple bond and the entrance channel of the reaction can be  
21 expected to be the same down to low temperatures as discussed by Goulay and coworkers.<sup>17</sup> It is  
22 therefore probable that reactions of the  $C_2H$  radical with  $C_4H_6$  molecules can contribute to  
23 molecular weight growth through the addition and subsequent elimination of a H-atom or methyl  
24 radical giving rise to  $C_5$  and  $C_6$  carbonaceous species. Diacetylene could also be a favorable exit  
25 channel.  
26  
27  
28  
29  
30  
31  
32  
33  
34  
35  
36

37 The distribution of  $C_6H_6$  isomers might be significantly altered at low temperatures. For instance,  
38 if thermal energy is required for isomerization of the initial adduct that leads to the formation of  
39 small 4- and 5-membered cyclic molecules, then this pathway could be disfavored at lower  
40 temperatures. However, the exothermicity of the reaction is substantial, and although Titan's  
41 atmosphere is cold, the low densities will limit collisional stabilization of intermediates; therefore  
42 most of the isomerization could still be enabled by chemical activation. Because of the numerous  
43 intermediates and transition states involved, with multiple product channels, further product  
44 detection studies of reactions involving the  $C_2H$  radical with  $C_4H_6$  isomers, especially at low  
45 temperatures, are required to have a detailed cartography of these radical-molecule reactions.  
46  
47  
48  
49  
50  
51  
52  
53  
54  
55  
56  
57  
58  
59  
60

## 5. Conclusion

Low temperature rate coefficients (74-295 K) for the  $C_2H + 1\text{-butyne}$  reaction are measured in a pulsed Laval nozzle apparatus. In this range, no apparent temperature dependence for the reaction is observed. This behavior is characteristic of a barrierless reaction at rates close to the collision limit, with the formation of an initial excited complex where the  $C_2H$  radical adds to the  $-C\equiv C-$  group of 1-butyne followed by either elimination of a hydrogen atom or methyl group. At room temperature, using Multiplexed Photoionization Mass Spectrometry, two competing product channels have been identified:  $m/z = 64$  ( $C_5H_4$ ) and  $m/z = 78$  ( $C_6H_6$ ) consistent with the  $CH_3-$  and H-loss channels for the reaction respectively. Ethynylallene is identified as the main linear  $C_5H_4$  isomer and is formed in a 4:1 ratio to methyldiacetylene. This result is consistent with the proposed reaction pathways where ethynylallene is most likely formed through a direct  $\beta$ -scission after terminal addition. Interestingly, the  $C_6H_6$  product channel yields cyclic isomers, i.e. fulvene and 3,4-dimethylenecyclobut-1-ene, in almost equal proportions to linear isomers. However, the most stable  $C_6H_6$  isomer, benzene, is most probably not produced in this reaction. Diacetylene formation is also thermodynamically possible, but its presence or absence cannot be ascertained in our experiment. Our results suggests that in the cold, photochemically driven atmosphere of Titan, the formation of linear  $C_6H_6$  isomers should be favored at the expense of cyclic structures due to significant isomerization barriers down the potential energy surface to resonance stabilized structures. The measured rate constants and product branching ratios constitute key laboratory data for the development of chemical schemes in devising more elaborate models for planetary atmospheres, and in particular Titan. Further experimental and theoretical investigations involving the  $C_2H$  radical with  $C_4$  carbonaceous species are required to have a detailed cartography of the potential energy surfaces for these reactions.

## Acknowledgement

The support of personnel (S.S.) for this research by the National Aeronautics and Space Administration (Grant No. NNX09AB60G) is gratefully acknowledged. We thank Mr. Howard Johnsen for excellent technical support. Sandia authors and instrumentation for this work are supported by the Division of Chemical Sciences, Geosciences and Biosciences, the Office of Basic Energy Sciences, the U.S. Department of Energy. Sandia is a multiprogram laboratory operated by Sandia Corporation, a Lockheed Martin Company, for the National Nuclear Security

1  
2  
3 Administration under Contract No. DE-AC04-94-AL85000. The Advanced Light Source and  
4 Chemical Sciences Division (K.R.W. and S.R.L.) are supported by the Director, Office of  
5 Science, Office of Basic Energy Sciences of the U.S. Department of Energy under Contract No.  
6 DE-AC02-05CH11231 at the Lawrence Berkeley National Laboratory. A.J.T. acknowledges  
7 travel funding provided by the International Synchrotron Access Program (ISAP) managed by the  
8 Australian Synchrotron. The ISAP is funded by a National Collaborative Research Infrastructure  
9 Strategy grant provided by the Federal Government of Australia.  
10  
11  
12  
13  
14  
15  
16  
17  
18  
19  
20  
21  
22  
23  
24  
25  
26  
27  
28  
29  
30  
31  
32  
33  
34  
35  
36  
37  
38  
39  
40  
41  
42  
43  
44  
45  
46  
47  
48  
49  
50  
51  
52  
53  
54  
55  
56  
57  
58  
59  
60

## Bibliography

- (1) Tucker, K. D.; Kutner, M. L.; Thaddeus, P. *Astrophysical Journal* **1974**, *193*, L115.
- (2) Coustenis, A.; Bezdard, B. *Icarus* **1995**, *115*, 126.
- (3) Coustenis, A.; Bezdard, B.; Gautier, D. *Icarus* **1989**, *80*, 54.
- (4) Coustenis, A.; Bezdard, B.; Gautier, D.; Marten, A.; Samuelson, R. *Icarus* **1991**, *89*, 152.
- (5) Seki, K.; Okabe, H. *Journal of Physical Chemistry* **1993**, *97*, 5284.
- (6) Wilson, E. H.; Atreya, S. K. *Planetary and Space Science* **2003**, *51*, 1017.
- (7) Sagan, C.; Khare, B. N.; Thompson, W. R.; McDonald, G. D.; Wing, M. R.; Bada, J. L.; Tuan, V. D.; Arakawa, E. T. *Astrophysical Journal* **1993**, *414*, 399.
- (8) Cook, D. J.; Schlemmer, S.; Balucani, N.; Wagner, D. R.; Steiner, B.; Saykally, R. *J. Nature* **1996**, *380*, 227.
- (9) Snow, T. P.; Le Page, V.; Keheyan, Y.; Bierbaum, V. M. *Nature* **1998**, *391*, 259.
- (10) Coustenis, A.; Achterberg, R. K.; Conrath, B. J.; Jennings, D. E.; Marten, A.; Gautier, D.; Nixon, C. A.; Flasar, F. M.; Teanby, N. A.; Bezdard, B.; Samuelson, R. E.; Carlson, R. C.; Lellouch, E.; Bjoraker, G. L.; Romani, P. N.; Taylor, F. W.; Irwin, P. G. J.; Fouchet, T.; Hubert, A.; Orton, G. S.; Kunde, V. G.; Vinatier, S.; Mondellini, J.; Abbas, M. M.; Courtin, R. *Icarus* **2007**, *189*, 35.
- (11) Mebel, A. M.; Kislov, V. V.; Kaiser, R. I. *Journal of the American Chemical Society* **2008**, *130*, 13618.
- (12) Wang, H.; Frenklach, M. *Combustion and Flame* **1997**, *110*, 173.
- (13) Carty, D.; Le Page, V.; Sims, I. R.; Smith, I. W. M. *Chemical Physics Letters* **2001**, *344*, 310.
- (14) Ceursters, B.; Nguyen, H. M. T.; Peeters, J.; Nguyen, M. T. *Chemical Physics Letters* **2000**, *329*, 412.
- (15) Ceursters, P.; Nguyen, H. M. T.; Peeters, J.; Nguyen, M. T. *Chemical Physics* **2000**, *262*, 243.
- (16) Goulay, F.; Leone, S. R. *Journal of Physical Chemistry A* **2006**, *110*, 1875.
- (17) Goulay, F.; Osborn, D. L.; Taatjes, C. A.; Zou, P.; Meloni, G.; Leone, S. R. *Physical Chemistry Chemical Physics* **2007**, *9*, 4291.
- (18) Hoobler, R. J.; Leone, S. R. *Journal of Geophysical Research-Planets* **1997**, *102*, 28717.
- (19) Hoobler, R. J.; Leone, S. R. *Journal of Physical Chemistry A* **1999**, *103*, 1342.
- (20) Landera, A.; Mebel, A. M.; Kaiser, R. I. *Chemical Physics Letters* **2008**, *459*, 54.
- (21) Lee, S.; Hoobler, R. J.; Leone, S. R. *Review of Scientific Instruments* **2000**, *71*, 1816.
- (22) Lee, S.; Samuels, D. A.; Hoobler, R. J.; Leone, S. R. *Journal of Geophysical Research-Planets* **2000**, *105*, 15085.
- (23) Stahl, F.; Schleyer, P. V.; Bettinger, H. F.; Kaiser, R. I.; Lee, Y. T.; Schaefer, H. F. *Journal of Chemical Physics* **2001**, *114*, 3476.
- (24) Vakhtin, A. B.; Heard, D. E.; Smith, I. W. M.; Leone, S. R. *Chemical Physics Letters* **2001**, *348*, 21.
- (25) Vakhtin, A. B.; Heard, D. E.; Smith, I. W. M.; Leone, S. R. *Chemical Physics Letters* **2001**, *344*, 317.

- 1  
2  
3 (26) Zhang, F. T.; Kim, S.; Kaiser, R. I. *Physical Chemistry Chemical Physics* **2009**,  
4 11, 4707.  
5 (27) Krasnopolsky, V. A. *Icarus* **2009**, 201, 226.  
6 (28) Yung, Y. L.; Allen, M.; Pinto, J. P. *Astrophysical Journal Supplement Series* **1984**,  
7 55, 465.  
8 (29) Hebrard, E.; Dobrijevic, M.; Benilan, Y.; Raulin, F. *Journal of Photochemistry*  
9 *and Photobiology C-Photochemistry Reviews* **2006**, 7, 211.  
10 (30) Hansmann, B.; Abel, B. *Chemphyschem* **2007**, 8, 343.  
11 (31) Dupeyrat, G.; Marquette, J. B.; Rowe, B. R. *Physics of Fluids* **1985**, 28, 1273.  
12 (32) Rowe, B. R.; Dupeyrat, G.; Marquette, J. B.; Gaucherel, P. *Journal of Chemical*  
13 *Physics* **1984**, 80, 4915.  
14 (33) Chastaing, D.; James, P. L.; Sims, I. R.; Smith, I. W. M. *Faraday Discussions*  
15 **1998**, 109, 165.  
16 (34) James, P. L.; Sims, I. R.; Smith, I. W. M.; Alexander, M. H.; Yang, M. B. *Journal*  
17 *of Chemical Physics* **1998**, 109, 3882.  
18 (35) Sims, I. R.; Smith, I. W. M. *Annual Review of Physical Chemistry* **1995**, 46, 109.  
19 (36) Atkinson, D. B.; Jaramillo, V. I.; Smith, M. A. *Journal of Physical Chemistry A*  
20 **1997**, 101, 3356.  
21 (37) Atkinson, D. B.; Smith, M. A. *Journal of Physical Chemistry* **1994**, 98, 5797.  
22 (38) Berteloite, C.; Le Picard, S. D.; Birza, P.; Gazeau, M. C.; Canosa, A.; Benilan, Y.;  
23 Sims, I. R. *Icarus* **2008**, 194, 746.  
24 (39) Nizamov, B.; Leone, S. R. *Journal of Physical Chemistry A* **2004**, 108, 1746.  
25 (40) Vuitton, V.; Doussin, J. F.; Benilan, Y.; Raulin, F.; Gazeau, M. C. *Icarus* **2006**,  
26 185, 287.  
27 (41) Vuitton, V.; Yelle, R. V.; Cui, J. *Journal of Geophysical Research-Planets* **2008**,  
28 113, 18.  
29 (42) Lavvas, P. P.; Coustenis, A.; Vardavas, I. M. *Planetary and Space Science* **2008**,  
30 56, 27.  
31 (43) Lavvas, P. P.; Coustenis, A.; Vardavas, I. M. *Planetary and Space Science* **2008**,  
32 56, 67.  
33 (44) Hansen, N.; Miller, J. A.; Kasper, T.; Kohse-Hoinghaus, K.; Westmoreland, P. R.;  
34 Wang, J.; Cool, T. A. *Proceedings of the Combustion Institute* **2009**, 32, 623.  
35 (45) Vanlook, H.; Peeters, J. *Journal of Physical Chemistry* **1995**, 99, 16284.  
36 (46) Montgomery, J. A.; Frisch, M. J.; Ochtanski, J. W.; Petersson, G. A. *Journal of*  
37 *Chemical Physics* **1999**, 110, 2822.  
38 (47) Montgomery, J. A.; Frisch, M. J.; Ochtanski, J. W.; Petersson, G. A. *Journal of*  
39 *Chemical Physics* **2000**, 112, 6532.  
40 (48) Ervin, K. M., PESCAL, Fortran program, 2009.  
41 (49) Ervin, K. M.; Ramond, T. M.; Davico, G. E.; Schwartz, R. L.; Casey, S. M.;  
42 Lineberger, W. C. *Journal of Physical Chemistry A* **2001**, 105, 10822.  
43 (50) Osborn, D. L.; Zou, P.; Johnsen, H.; Hayden, C. C.; Taatjes, C. A.; Knyazev, V.  
44 D.; North, S. W.; Peterka, D. S.; Ahmed, M.; Leone, S. R. *Review of Scientific Instruments* **2008**,  
45 79.  
46 (51) Slagle, I. R.; Yamada, F.; Gutman, D. *Journal of the American Chemical Society*  
47 **1981**, 103, 149.  
48 (52) Meloni, G.; Selby, T. M.; Goulay, F.; Leone, S. R.; Osborn, D. L.; Taatjes, C. A.  
49 *Journal of the American Chemical Society* **2007**, 129, 14019.  
50  
51  
52  
53  
54  
55  
56  
57  
58  
59  
60

- 1  
2  
3 (53) Minsek, D. W.; Chen, P. *Journal of Physical Chemistry* **1990**, *94*, 8399.  
4 (54) Bieri, G.; Burger, F.; Heilbronner, E.; Maier, J. P. *Helvetica Chimica Acta* **1977**,  
5 60, 2213.  
6 (55) Kiess, N. H.; Broida, H. P. *Astrophysical Journal* **1956**, *123*, 166.  
7 (56) Cvejanovic, D.; Adams, A.; King, G. C. *Journal of Physics B-Atomic Molecular*  
8 *and Optical Physics* **1978**, *11*, 1653.  
9 (57) Sander, R. K.; Tsee, J. J.; Quick, C. R.; Romero, R. J. *Journal of Chemical Physics*  
10 **1988**, *89*, 3495.  
11 (58) Nakayama, T.; Watanabe, K. *Journal of Chemical Physics* **1964**, *40*, 558.  
12 (59) Laufer, A. H.; Fahr, A. *Chem. Rev.* **2004**, *104*, 2813.  
13 (60) Berkowitz, J.; Ellison, G. B.; Gutman, D. *Journal of Physical Chemistry* **1994**, *98*,  
14 2744.  
15 (61) Miller, J. A.; Klippenstein, S. J. *Journal of Physical Chemistry A* **2003**, *107*, 7783.  
16 (62) Hansen, N.; Klippenstein, S. J.; Miller, J. A.; Wang, J.; Cool, T. A.; Law, M. E.;  
17 Westmoreland, P. R.; Kasper, T.; Kohse-Hoinghaus, K. *Journal of Physical Chemistry A* **2006**,  
18 *110*, 4376.  
19 (63) Bobeldijk, M.; Vanderzande, W. J.; Kistemaker, P. G. *Chemical Physics* **1994**,  
20 *179*, 125.  
21 (64) Fahr, A.; Selby, T. M.; Osborn, D. L.; Taatjes, C. A. private communication, 2006.  
22 (65) Nemeth, G. I.; Selzle, H. L.; Schlag, E. W. *Chemical Physics Letters* **1993**, *215*,  
23 151.  
24 (66) Rosenstock, H. M.; Dannacher, J.; Liebman, J. F. *Radiation Physics and*  
25 *Chemistry* **1982**, *20*, 7.  
26 (67) Masclet, P.; Mouvier, G.; Bocquet, J. F. *Journal De Chimie Physique Et De*  
27 *Physico-Chimie Biologique* **1981**, *78*, 99.  
28 (68) Beez, M.; Bieri, G.; Bock, H.; Heilbron, E. *Helvetica Chimica Acta* **1973**, *56*, 1028.  
29 (69) Goulay, F.; Rebrion-Rowe, C.; Biennier, L.; Le Picard, S. D.; Canosa, A.; Rowe,  
30 B. R. *Journal of Physical Chemistry A* **2006**, *110*, 3132.  
31 (70) Herbst, E.; Woon, D. E. *Astrophysical Journal* **1997**, *489*, 109.  
32 (71) Senosiain, J. P.; Miller, J. A. *Journal of Physical Chemistry A* **2007**, *111*, 3740.  
33 (72) Matheu, D. M.; Green, W. H.; Grenda, J. M. *International Journal of Chemical*  
34 *Kinetics* **2003**, *35*, 95.  
35 (73) Laufer, A. H.; Fahr, A. *Chemical Reviews* **2004**, *104*, 2813.  
36 (74) Woon, D. E.; Park, J. Y. *Icarus* **2009**, *202*, 642.  
37 (75) Maier, J. P. *Angewandte Chemie-International Edition in English* **1981**, *20*, 638.  
38 (76) Hayaishi, T.; Iwata, S.; Sasanuma, M.; Ishiguro, E.; Morioka, Y.; Iida, Y.;  
39 Nakamura, M. *Journal of Physics B-Atomic Molecular and Optical Physics* **1982**, *15*, 79.  
40  
41  
42  
43  
44  
45  
46  
47  
48  
49  
50  
51  
52  
53  
54  
55  
56  
57  
58  
59  
60

## Captions for Figures:

Figure 1: (a) Example of net CH ( $A^2\Delta - X^2\Pi_r$ ) chemiluminescence decay signal at 431.22 nm<sup>56</sup> on a linear scale, and (b) a semi-logarithmic scale. The solid black line is the single exponential fit of the signal within the range 15 – 200  $\mu$ s as indicated by the dashed line. The chemiluminescence signal is proportional to the concentration of ethynyl radicals ( $C_2H$ ) under the experimental conditions.

Figure 2: Plot of the pseudo first order rate constant ( $k_{obs}$ ) as a function of the density of 1-butyne inside the flow at 84 K and 0.3 Torr. The black line is a least squares fit to the experimental values. The error bars are given as  $\pm 2\sigma$  of the single exponential fits for each concentration.

Figure 3: Mass spectra at 10.1 eV photoionization energy with (a) the  $C_2H$  precursor and 1-butyne and (b) only 1-butyne flowing under the same exact conditions. Two masses show a significant rise as the  $C_2H$  precursor is added, i.e.  $m/z = 64$  and  $m/z = 78$  which are consistent with the  $CH_3$ - and H-loss channels of the reaction respectively. The contribution of the 193 nm photoproducts of 1-butyne to the  $m/z = 78$  product channel of the reaction is discussed in Section 3.2.1. Note that the contribution to the ion signal at  $m/z = 66$  ( $\star$ ) is due to the reaction of the ethynyl radical with butene ( $C_4H_8$ ) present as a small contaminant in the flow.

Figure 4: Photoionization efficiency curves for  $m/z = 78$  ( $C_6H_6$ ) mass channel with ( $\blacklozenge$ ) and without ( $\otimes$ ) the  $C_2H$  precursor. Both PIE curves have been recorded with the same concentration of 1-butyne in the total gas flow. The photodissociation of 1-butyne at 193 nm produces propargyl radicals ( $C_3H_3$ ) that subsequently react with 1-butyne to form  $C_6H_6 + CH_3$ . In presence of  $C_2H$  radicals, the ion signal is enhanced (typically by a factor of  $\sim 6$ ) which is consistent with the formation of  $C_6H_6$  as a product of the reaction of  $C_2H$  radicals with 1-butyne. Two thresholds are identified and indicated by dashed arrows: (A) around 8.8 eV photoionization energy as shown in the region between 8.1 and 8.9 eV (zoom x8) and (B) around 9.4 eV. The identification of the different isomers  $C_6H_6$  is discussed in Section 3.2.3.



1  
2  
3  
4  
5 Figure 5: Measurements of the photodepletion of (a) 1-butyne, (b) acetylene and (c) 3,3,3-  
6 trifluoropropyne at 193 nm. All gases are seeded in He buffer gas at the following compositions:  
7 0.1 % for both 1-butyne and acetylene and 1% for 3,3,3-trifluoropropyne. The excimer laser  
8 energy used for the three different species is typically  $\sim 27 \text{ mJ/cm}^2$ . All data sets are fit by a step  
9 function (solid black line) after the laser is pulsed at 20 ms. The percentage depletion is reported  
10 in Table 4.  
11  
12  
13  
14  
15  
16

17 Figure 6: Photoionization efficiency curve ( $\oplus$ ) of  $m/z = 78$  product ion. The individual  
18 contributions of the  $\text{C}_6\text{H}_6$  isomers (dotted and dashed lines) are shown, as well as the cumulative  
19 simulation (thick black line). The adiabatic ionization energies for each isomer are also labeled:  
20 (a) fulvene, (b) DMCB, (c) 2-ethynyl-1,3-butadiene, 3,4-hexadiene-1-yne and (d) 1,3-hexadiyne.  
21 The production of the aromatic 6-membered ring isomer, benzene, is most probably negligible as  
22 no sharp characteristic onset is observed around 9.23 eV (see Section 3.2.3). The PIE curve is  
23 normalized to the total estimated cross section of an average mixture of 18% of fulvene, 32% of  
24 DMCB, 8% of 2-ethynyl-1,3-butadiene, 28% of 3,4-hexadiene-1-yne and 14% of 1,3-hexadiyne  
25 using the estimated photoionization cross sections at 10 eV reported in Table 6.  
26  
27  
28  
29  
30  
31  
32  
33

34 Figure 7: Photoionization efficiency curve ( $\oplus$ ) of  $m/z = 64$ . Note that no threshold in the ion  
35 signal is observed at 8.67 eV, indicating that no 1,2,3,4-pentatetraene is produced in the reaction.  
36 (a) A single contribution of ethynylallene cannot account for the observed ion signal in the 8.2 –  
37 10.1 photon range. (b) The individual contributions of ethynylallene (dashed line) and  
38 methyldiacetylene (dotted line) are shown. The ion signal can be fit by a sum of weighted  
39 contributions of Franck-Condon simulations<sup>62</sup> at 300 K of the two most stable  $\text{C}_5\text{H}_4$  isomers as  
40 shown by the thick black line. The calculated PIE curve of 1,4-pentadiyne (gray dashed line) is  
41 also indicated. Due to experimental limitations, the presence or absence of 1,4-pentadiyne (IE =  
42 10.27 eV)<sup>62</sup> cannot be probed. The signal is normalized to the total estimated photoionization  
43 cross section at 9.8 eV using estimated values reported in Table 5.  
44  
45  
46  
47  
48  
49  
50  
51  
52  
53  
54  
55  
56  
57  
58  
59  
60

1  
2  
3 Figure 8: Comparison between the measured rate constant for the reactions of the ethynyl radical  
4 with 1-butyne (<sup>a</sup>this work) and the smaller alkynes: propyne (<sup>b</sup>Leone and coworkers<sup>25</sup> and <sup>c</sup>Sims  
5 and coworkers<sup>13</sup>) and acetylene (<sup>d</sup>Leone and coworkers<sup>24</sup> and <sup>e</sup>Sims and coworkers<sup>33</sup>).  
6  
7  
8

9  
10 Figure 9: A comparison of the thermochemistry of the  $C_3H_3 + C_3H_3$  and  $C_2H + 1$ -butyne  
11 reactions. The standard heats of reaction (kcal/mol) leading to the three most stable  $C_6H_6$   
12 isomers, i.e. DMCB, fulvene and benzene respectively are shown in both cases. The difference in  
13 internal energy accompanying benzene is  $\sim 38$  kcal/mol. The exothermicity of the  $CH_3$ - and  $C_2H_5$ -  
14 loss channels forming methyldiacetylene ( $CH_3CCCCH$ ) and diacetylene ( $HCCCCH$ ) respectively  
15 is also shown.  
16  
17  
18  
19

20  
21 Figure 10: Proposed reaction pathways following addition of  $C_2H$  radical (shown in bold  
22 characters) to the terminal acetylenic carbon atom in 1-butyne. The initial adduct formed is  
23 shown inside the rectangular frame.  
24  
25  
26  
27

28  
29 Figure 11: Proposed reaction pathways following addition of the  $C_2H$  radical (shown in bold  
30 characters) to the central acetylenic carbon atom in 1-butyne. The initial adduct formed is shown  
31 inside the rectangular frame.  
32  
33  
34  
35  
36  
37  
38  
39  
40  
41  
42  
43  
44  
45  
46  
47  
48  
49  
50  
51  
52  
53  
54  
55  
56  
57  
58  
59  
60

## Captions for Tables:

Table 1: Isomers of  $C_6H_6$  relevant to this work and their ionization energies.

Table 2: Isomers of  $C_5H_4$  relevant to this work and their ionization energies.

Table 3: Low temperature rate coefficients of the reaction of the ethynyl radical ( $C_2H$ ) with 1-butyne ( $C_4H_6$ ) obtained with the pulsed Laval nozzle apparatus. The values are given with a total uncertainty of 20%.

Table 4: Percent photo-depletion of acetylene, 3,3,3-trifluoropropyne and 1-butyne at 193 nm at a laser energy  $\sim 27$  mJ/pulse. The experimental data is fit to a step function after the laser is pulsed, i.e. at  $t = 20$  ms (see Figure 5 and Section 3.2.1).

Table 5: Estimated photoionization absorption cross sections of  $C_5H_4$  isomers identified in the PIE curve shown in Figure 7 (see Section 3.2.2).

Table 6: Estimated photoionization absorption cross sections of  $C_6H_6$  isomers (see Section 3.2.3) identified in the PIE curve shown in Figure 6.

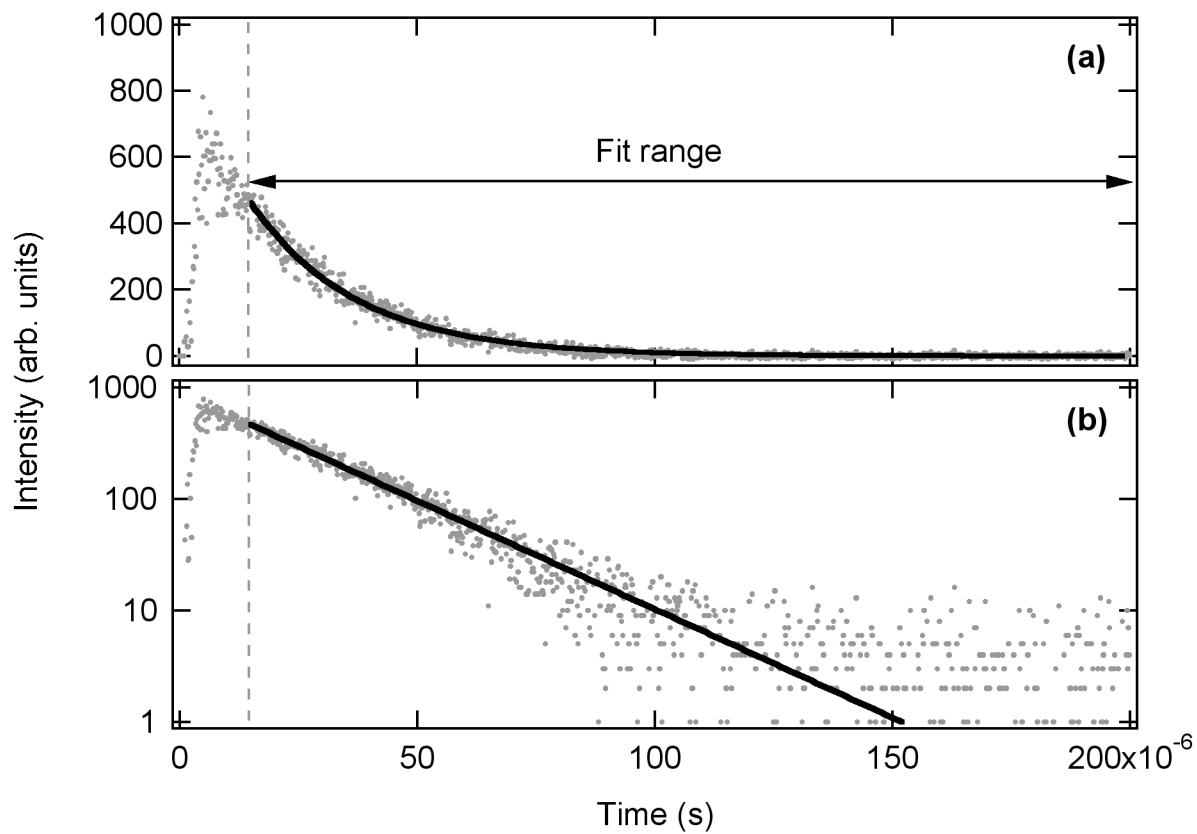


Figure 1

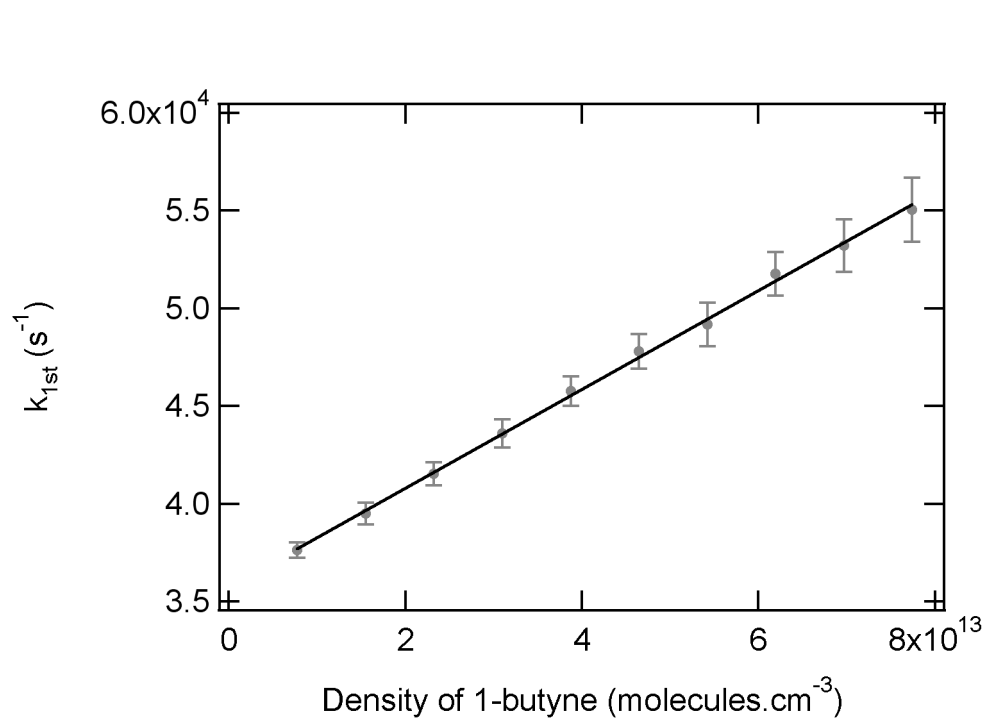


Figure 2

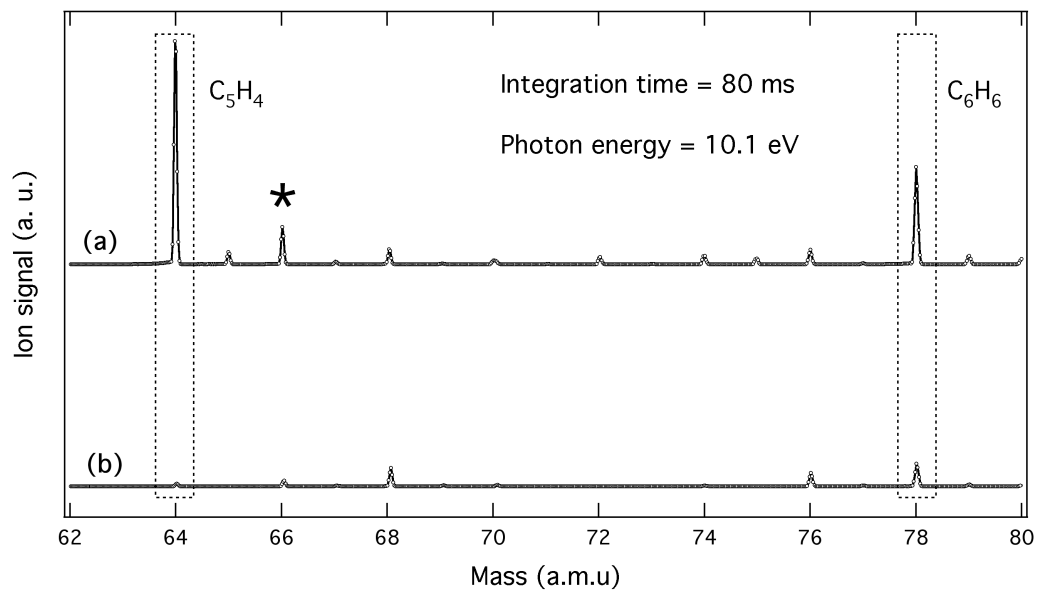


Figure 3

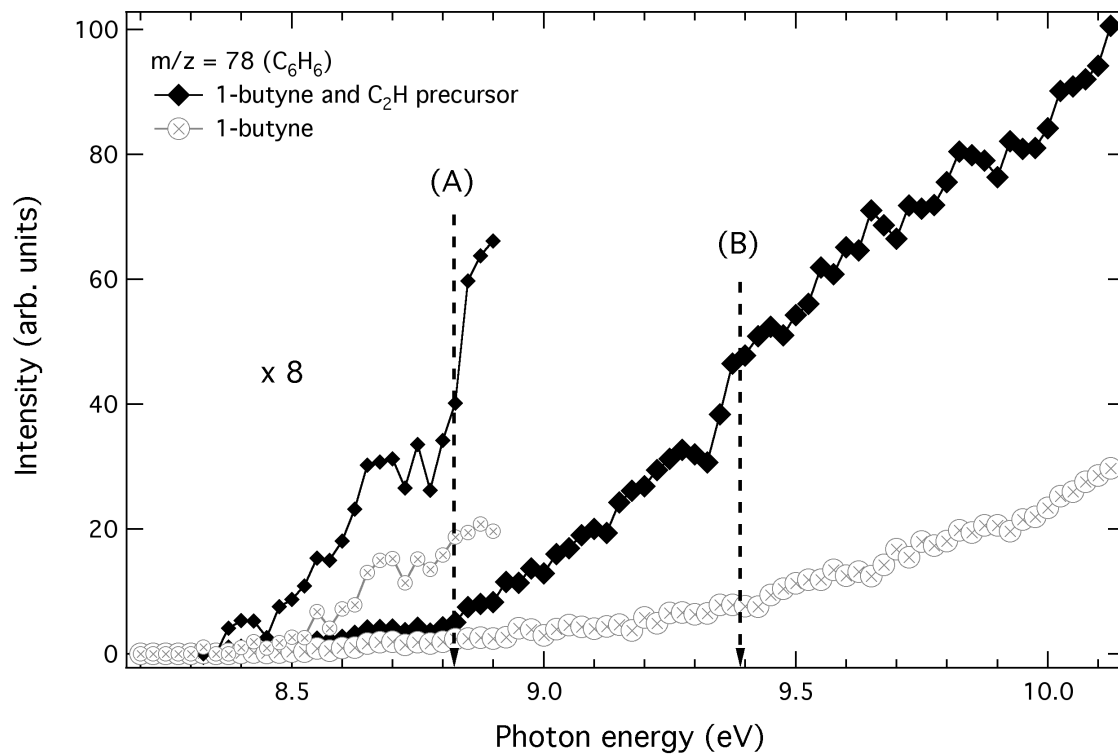


Figure 4

1  
2  
3  
4  
5  
6  
7  
8  
9  
10  
11  
12  
13  
14  
15  
16  
17  
18  
19  
20  
21  
22  
23  
24  
25  
26  
27  
28  
29  
30  
31  
32  
33  
34  
35  
36  
37  
38  
39  
40  
41  
42  
43  
44  
45  
46  
47  
48  
49  
50  
51  
52  
53  
54  
55  
56  
57  
58  
59  
60

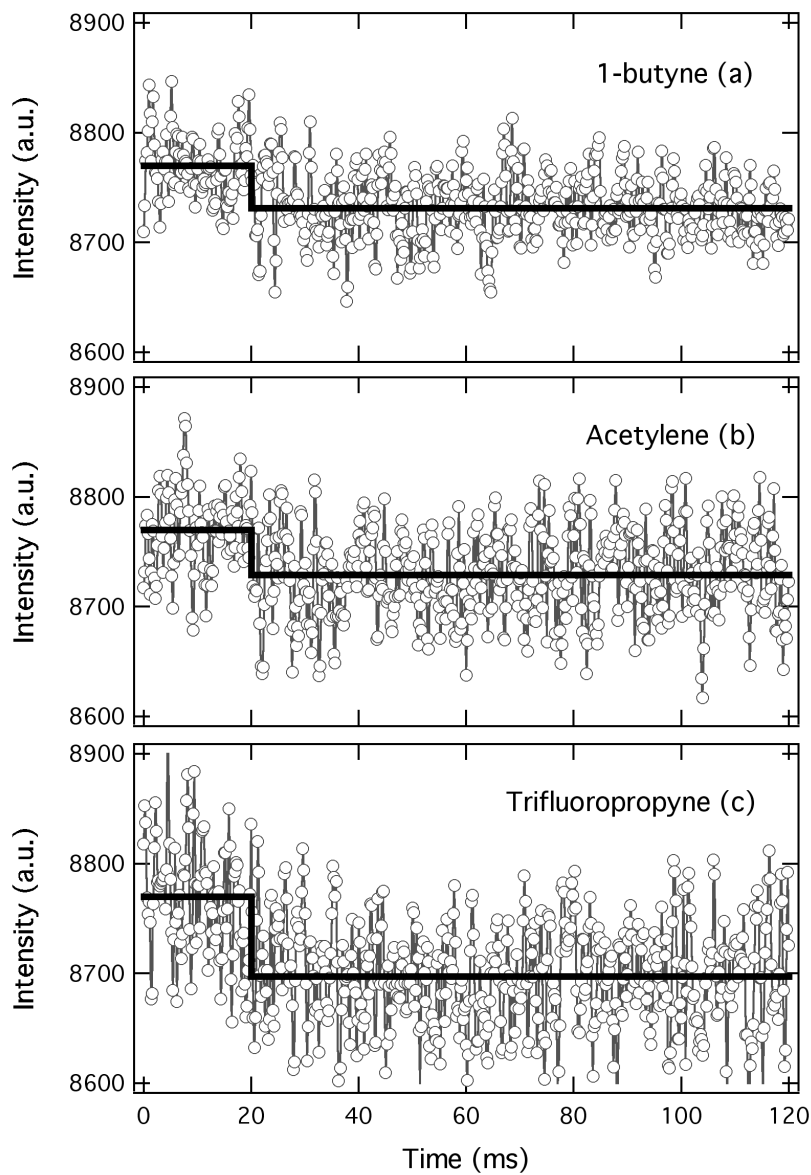


Figure 5



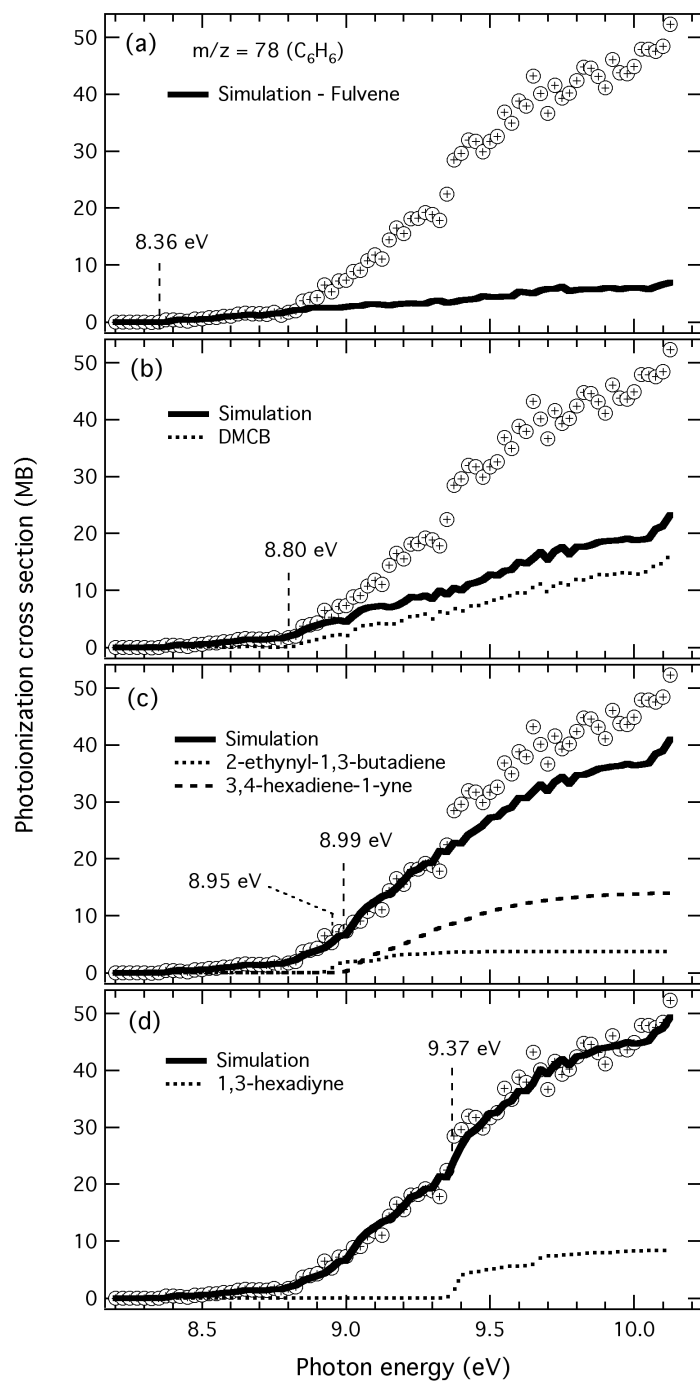


Figure 6

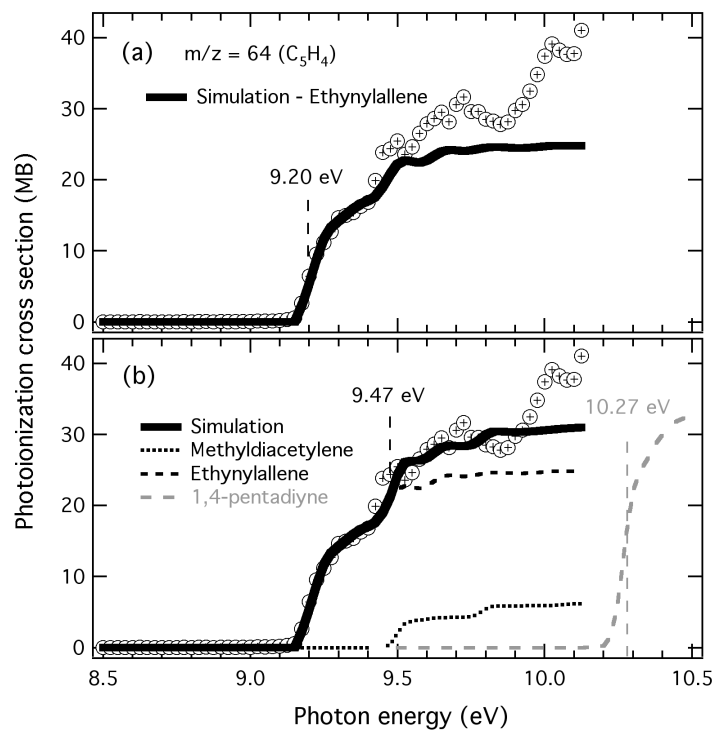


Figure 7

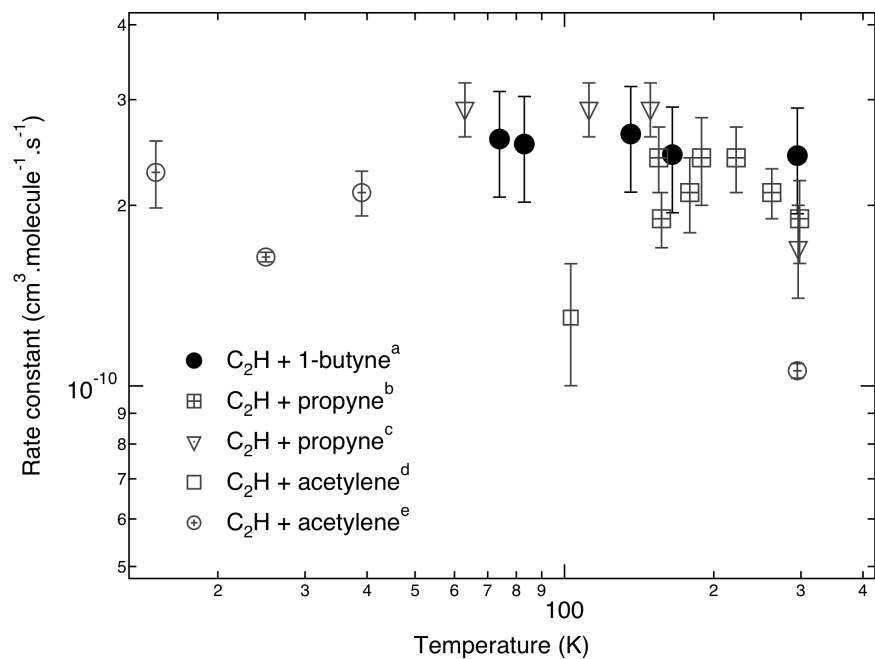


Figure 8

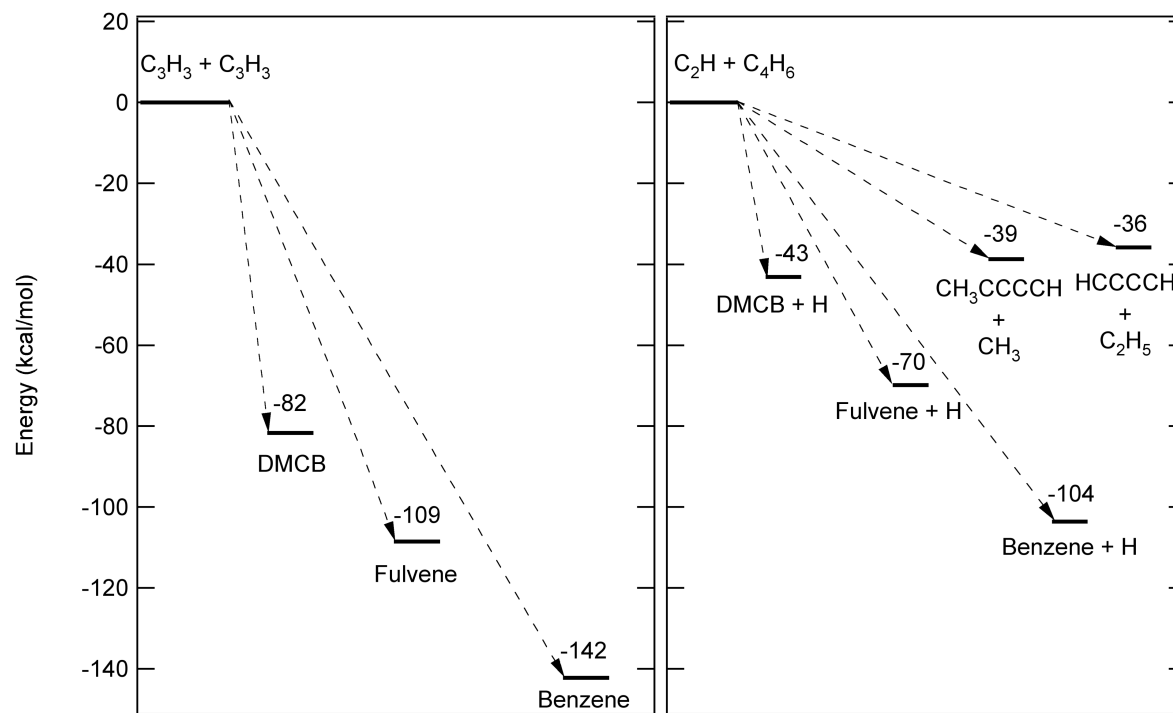


Figure 9

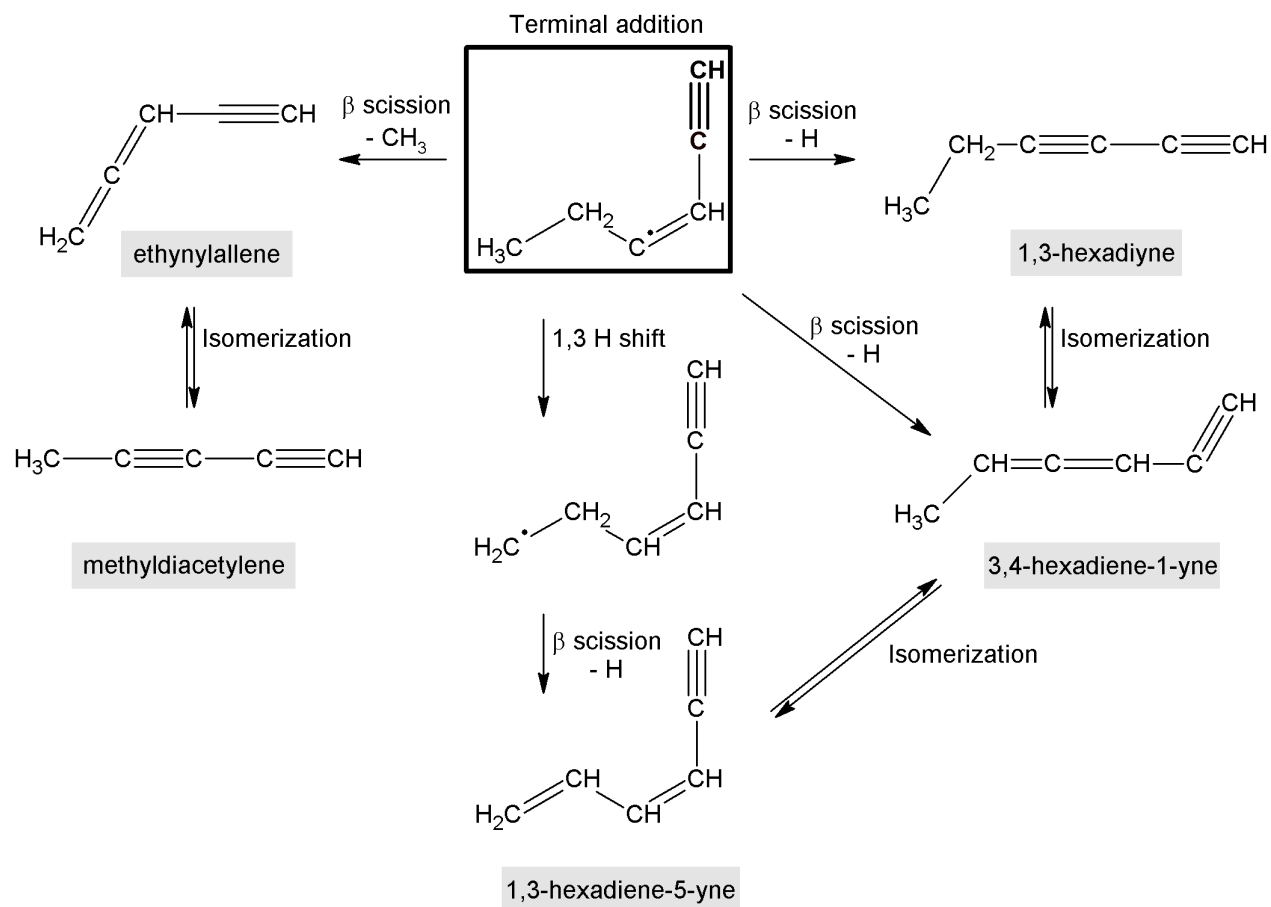


Figure 10

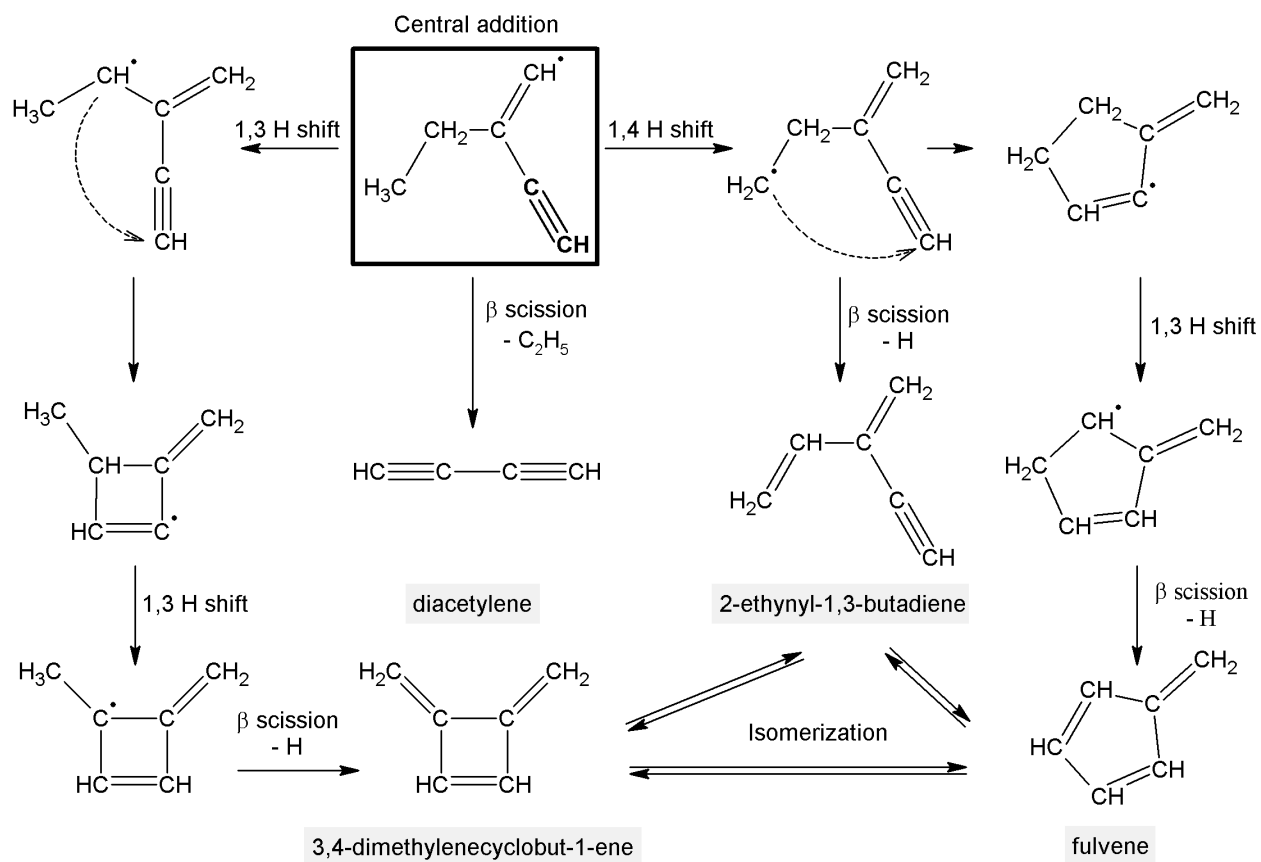
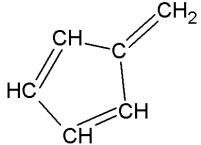
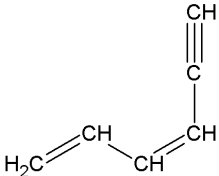
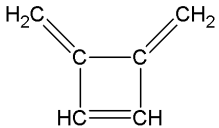
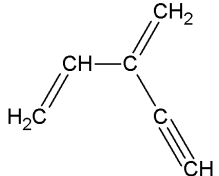
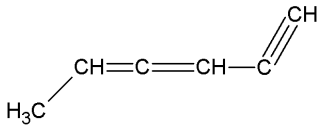
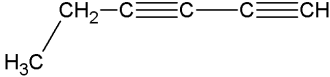
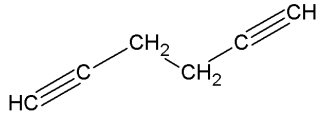


Figure 11

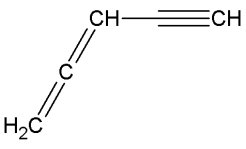
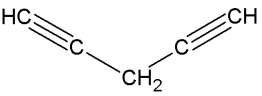
33  
34  
35  
36  
37  
38  
39  
40  
41  
42  
43  
44  
45  
46  
47  
48  
49  
50  
51  
52  
53  
54  
55  
56  
57  
58  
59  
60

Table 1

| Name                    | Molecular structure   | Ionization energies (eV) |                    |
|-------------------------|---|--------------------------|--------------------|
|                         |   | Calc. <sup>a</sup>       | Exp.               |
| Fulvene                 |    | 8.40                     | 8.36 <sup>b</sup>  |
| 1,3-hexadiene-5-yne     |    | 8.63                     | 9.2 <sup>c,d</sup> |
| DMCB                    |    | 8.75                     | 8.80 <sup>b</sup>  |
| 2-ethynyl-1,3-butadiene |   | 8.95                     |                    |
| 3,4-hexadiene-1-yne     |  | 8.99                     |                    |
| 1,3-hexadiyne           |  | 9.37                     | 9.41 <sup>c</sup>  |
| 1,5-hexadiyne           |  | 9.90                     | 9.90 <sup>b</sup>  |

<sup>a</sup>This work, CBS-QB3 calculations<sup>b</sup>Ref.<sup>54</sup><sup>c</sup>Ref.<sup>66</sup><sup>d</sup>Electron impact value minus 0.3 eV as reported in Ref.<sup>66</sup>

Table 2

| Name                  | Molecular structure   | Ionization energies (eV) |                    |
|-----------------------|---|--------------------------|--------------------|
|                       |   | Calc. <sup>a</sup>       | Lit.               |
| 1,2,3,4-pentatetraene | $\text{H}_2\text{C}=\text{C}=\text{C}=\text{C}=\text{CH}_2$                       |                          | 8.67 <sup>b</sup>  |
| ethynylallene         |  | 9.20                     | 9.22 <sup>c</sup>  |
| methyldiacetylene     | $\text{H}_3\text{C}-\text{C}\equiv\text{C}-\text{C}\equiv\text{CH}$               | 9.47                     | 9.5 <sup>d</sup>   |
| 1,4-pentadiyne        |  | 10.27                    | 10.28 <sup>c</sup> |

<sup>a</sup>This work, CBS-QB3 calculations<sup>b</sup>Ref.<sup>54</sup><sup>c</sup>Ref.<sup>62</sup><sup>d</sup>Ref.<sup>75</sup>



Table 3

| T<br>(K) | Total gas density<br>( $10^{16} \text{ cm}^{-3}$ ) | [C <sub>2</sub> H <sub>2</sub> ]<br>( $10^{14} \text{ cm}^{-3}$ ) | [O <sub>2</sub> ]<br>( $10^{14} \text{ cm}^{-3}$ ) | [1-butyne]<br>( $10^{12} \text{ cm}^{-3}$ ) | Rate constant<br>( $10^{-10} \text{ cm}^3 \text{ s}^{-1}$ ) |
|----------|--|---|--|---|---|
| 74       | 2.1  | 1.2   | 2.3  | 4.6 – 46                                    | 2.58±0.5  |
| 84       | 3.6  | 2.0   | 3.9  | 7.8 – 77                                    | 2.53±0.5  |
| 136      | 5.6  | 3.5   | 7.0  | 14 – 136                                    | 2.63±0.5  |
| 165      | 4.6  | 4.8   | 4.8  | 7.5 – 194                                   | 2.43±0.5  |
| 295      | 3.2  | 3.8   | 3.8  | 4.0 – 40                                    | 2.42±0.5  |

**Table 4**

| Molecule               | Formula                          | IE (eV)             | % in He buffer gas | % depletion |
|------------------------|----------------------------------|---------------------|--------------------|-------------|
| acetylene              | C <sub>2</sub> H <sub>2</sub>    | 11.40 <sup>76</sup> | 0.1                | 0.47        |
| 3,3,3-trifluoropropyne | CF <sub>3</sub> C <sub>2</sub> H | 11.96 <sup>54</sup> | 1.0                | 0.83        |
| 1-butyne               | C <sub>4</sub> H <sub>6</sub>    | 10.20 <sup>54</sup> | 0.1                | 0.45        |

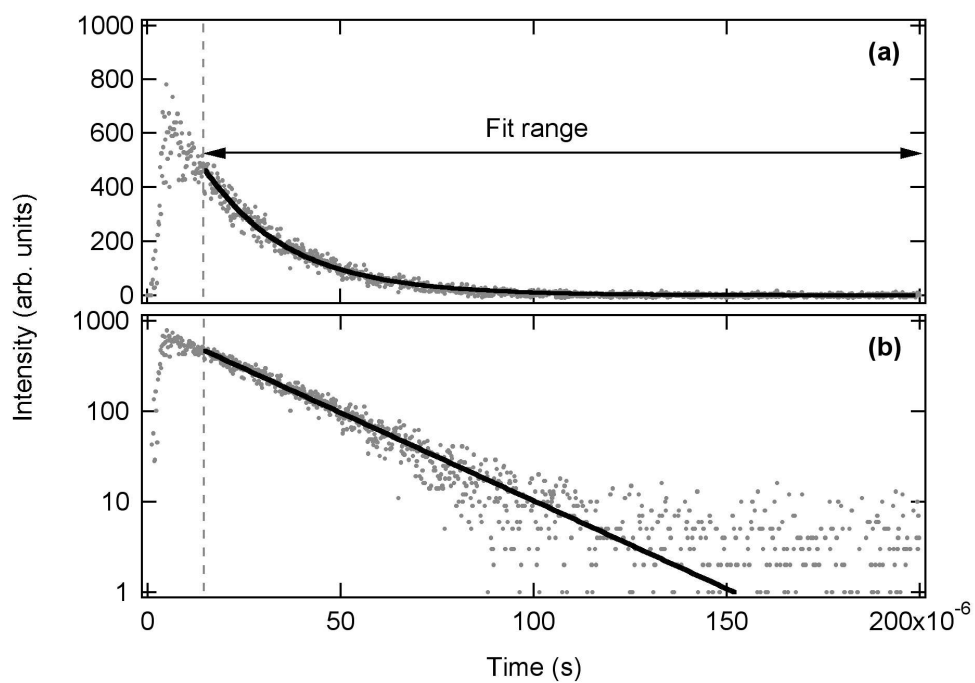
**Table 5**

| C <sub>5</sub> H <sub>4</sub> isomers | Photon energy (eV) |       |       |
|---------------------------------------|--------------------|-------|-------|
|                                       | 9.4                | 9.8   | 10.4  |
| ethynylallene <sup>a</sup>            | 25 MB              | 30 MB | 30 MB |
| methyldiacetylene <sup>a</sup>        |                    | 30 MB | 35 MB |
| 1,4-pentadiyne <sup>a</sup>           |                    |       | 30 MB |

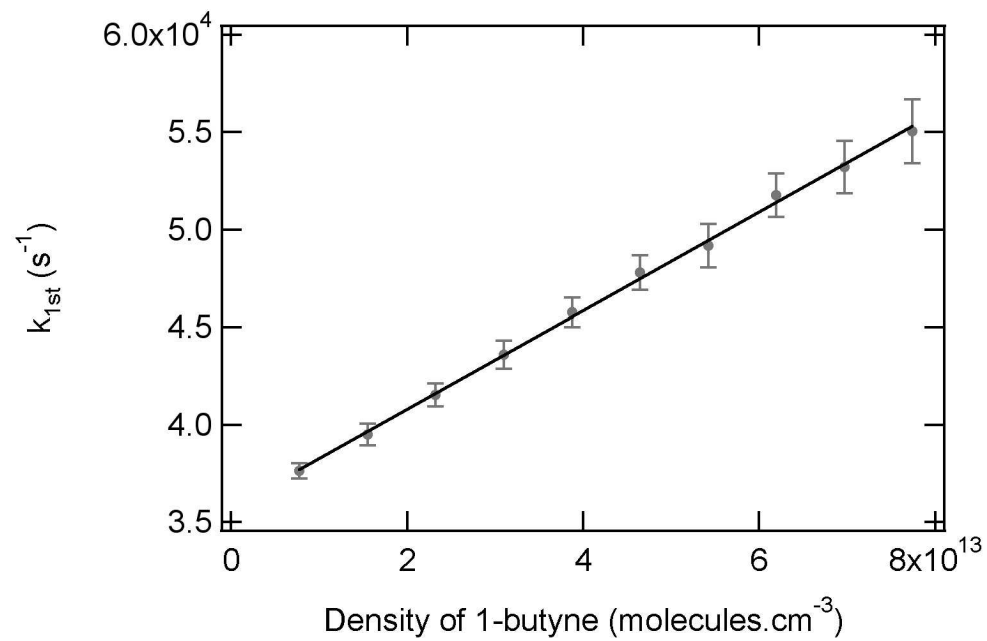
<sup>a</sup>Ref.<sup>17</sup>

**Table 6**

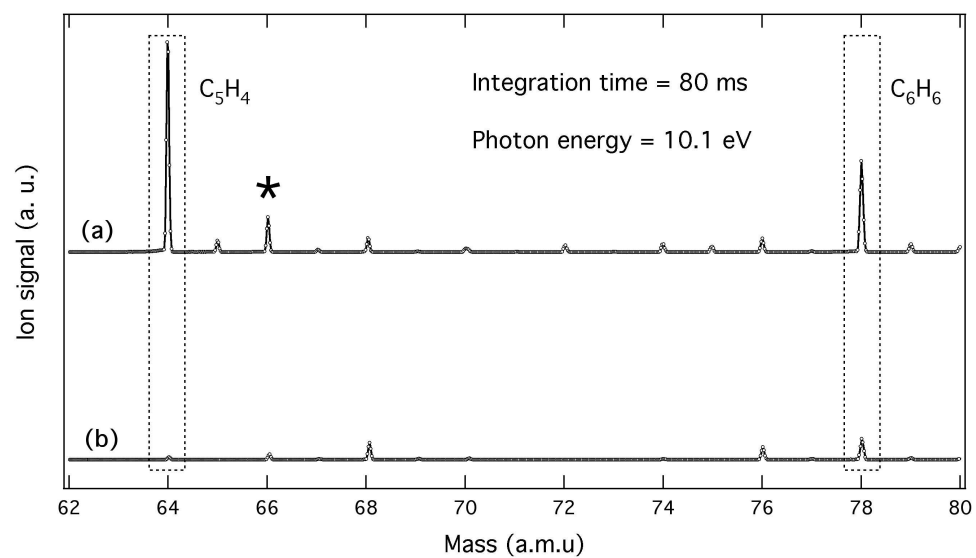
| C <sub>6</sub> H <sub>6</sub> isomers | Photon energy (eV) |       |       |       |
|---------------------------------------|--------------------|-------|-------|-------|
|                                       | 8.6                | 8.9   | 9.2   | 10    |
| fulvene                               | 6 MB               | 14 MB | 18 MB | 35 MB |
| 3,4-dimethylenecyclobut-1-ene         |                    | 5 MB  | 15 MB | 40 MB |
| 2-ethynyl-1,3-butadiene               |                    |       | 42 MB | 50 MB |
| 3,4-hexadiene-1-yne                   |                    |       | 18 MB | 50 MB |
| 1,3-hexadiyne                         |                    |       |       | 59 MB |



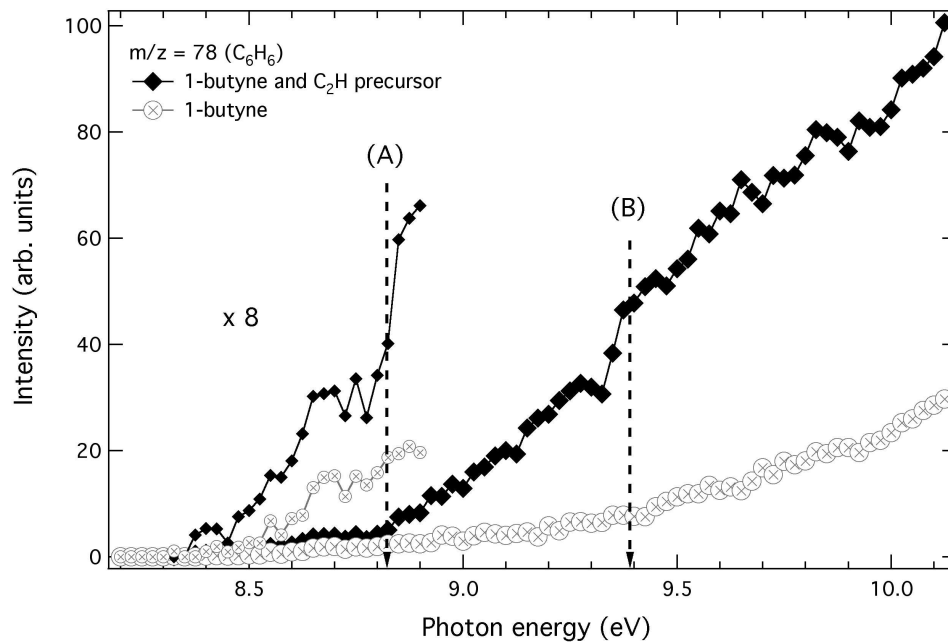
162x114mm (300 x 300 DPI)



132x84mm (300 x 300 DPI)

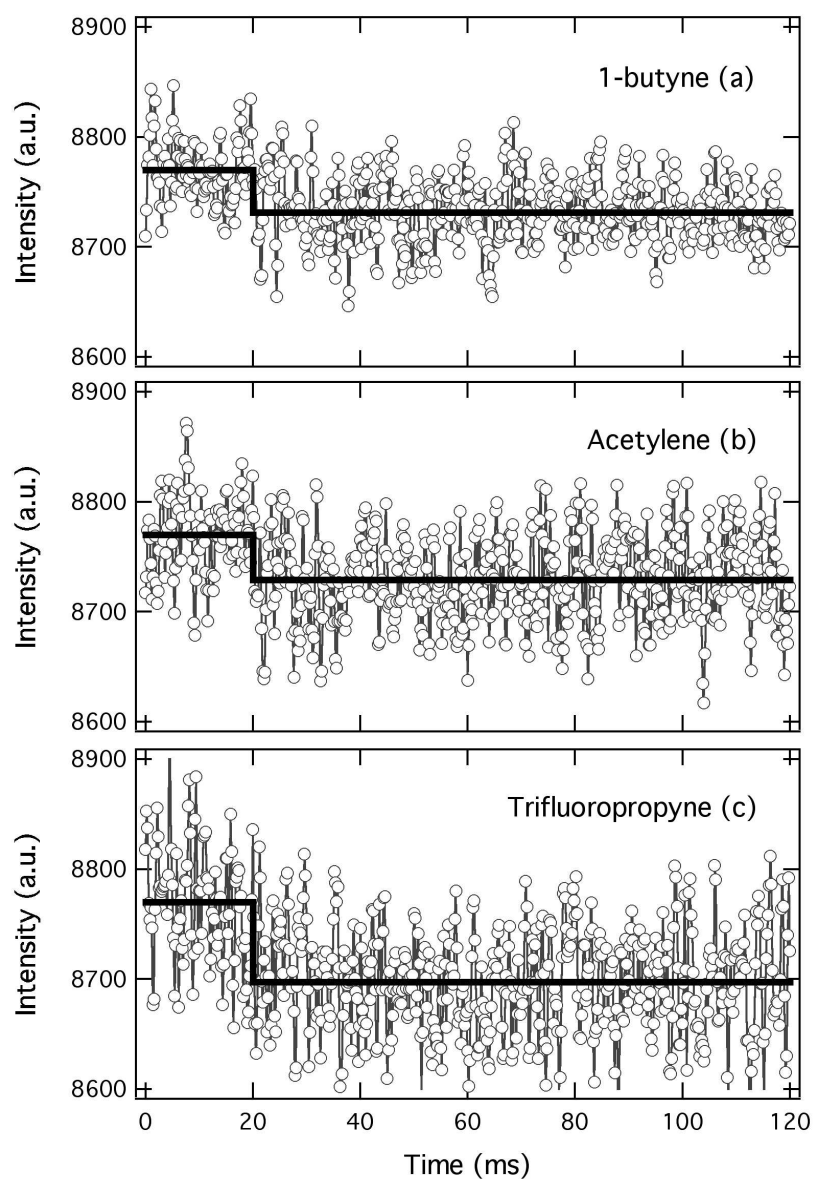


234x131mm (300 x 300 DPI)

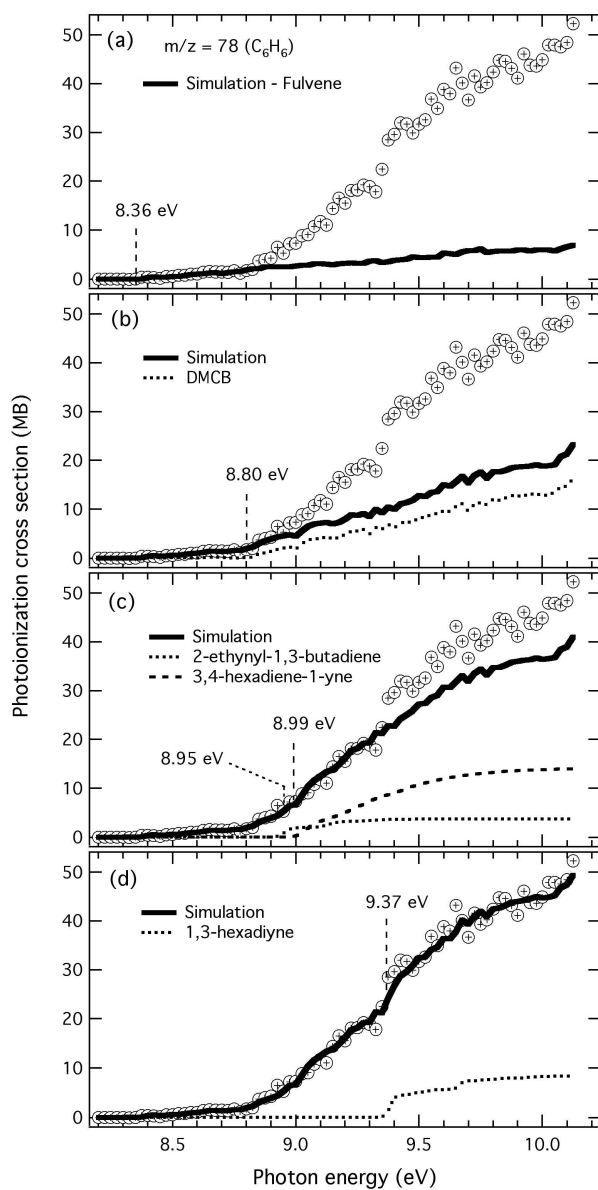


221x142mm (300 x 300 DPI)

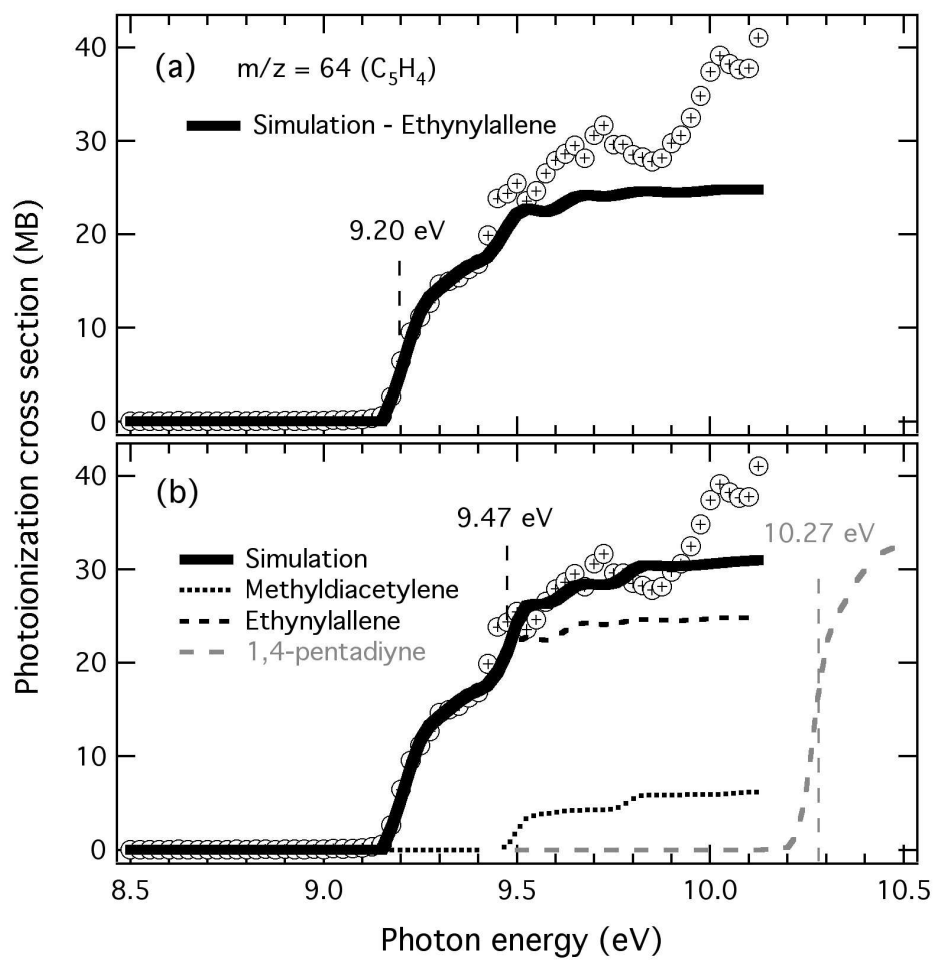




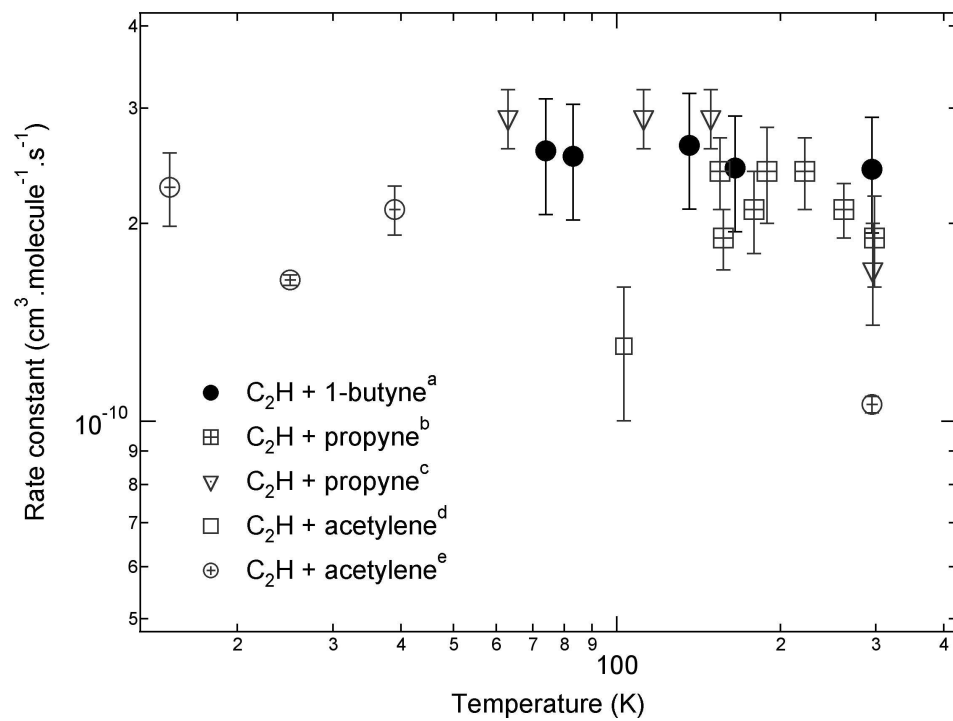
143x198mm (300 x 300 DPI)



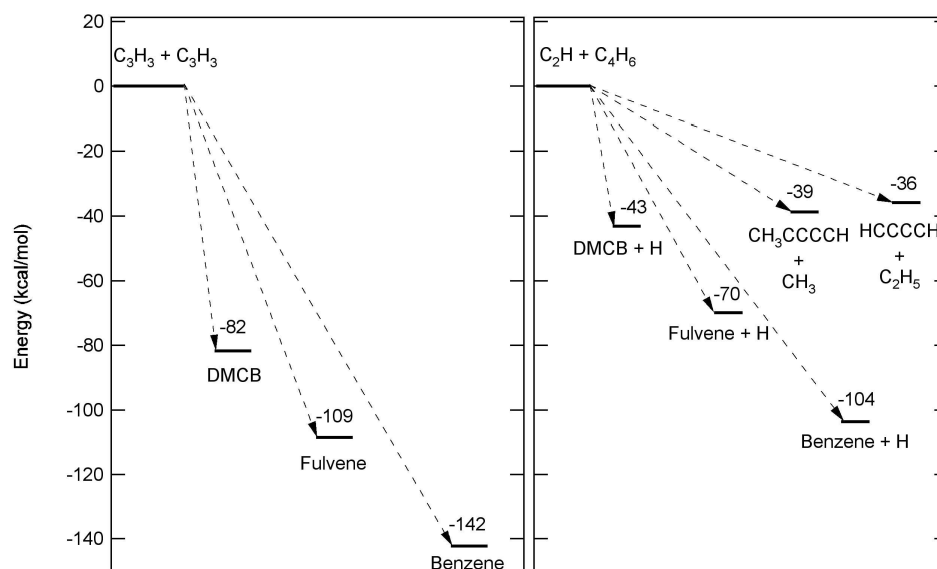
143x263mm (300 x 300 DPI)



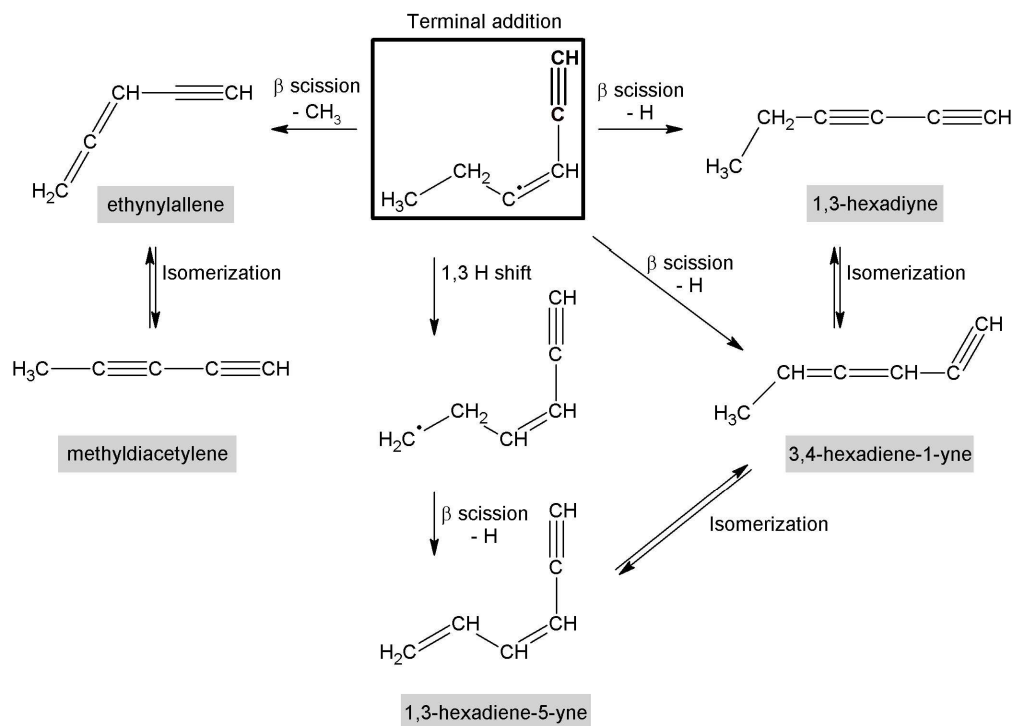
143x140mm (300 x 300 DPI)



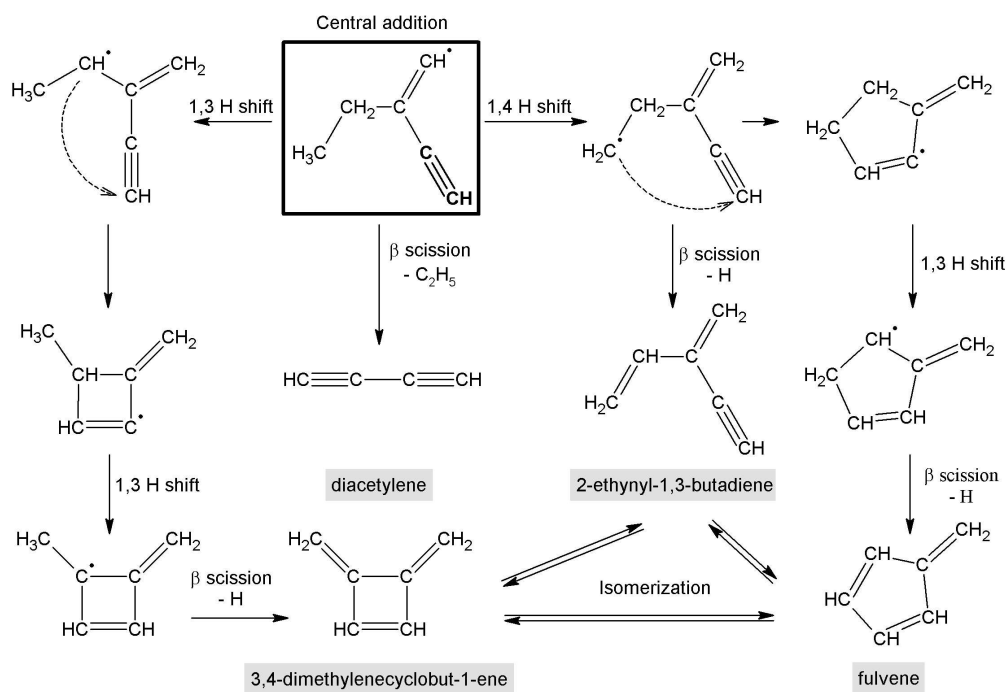
202x145mm (300 x 300 DPI)



226x149mm (300 x 300 DPI)



176x127mm (300 x 300 DPI)



189x128mm (300 x 300 DPI)